INVESTIGATION OF AN OSCILLATING WATER COLUMN CHAMBER USING COMMERCIAL CFD SOFTWARE

by

Endre Bozsó
D8ISGN

Submitted to the
Department of Fluid Mechanics of the
Budapest University of Technology and Economics
in partial fulfillment of the requirements for the degree of
Bachelor of Science in Mechanical Engineering

on the 13th of December, 2019

BSc Thesis

Final Project /BMEGEÁTA4SD/

Supervisor:
Csaba Horváth, PhD associate professor
Josh Davidson, PhD

Department of Fluid Mechanics
Faculty of Mechanical Engineering
Budapest University of Technology and Economics

DECLARATION

Full Name (as in ID):	Endre BOZSÓ
Neptun Code:	D8ISGN
University:	Budapest University of Technology and Economics
Faculty:	Faculty of Mechanical Engineering
Department:	Department of Fluid Mechanics
Minor:	BSc in Mechanical Engineering Spec. in Process Engineering (2N-AG0-FT)
BSc Thesis title:	Investigation of an Oscillating Water Column (OWC) chamber using commercial CFD software
Academic year of submission:	2019/2020/1

I, the undersigned, hereby declare that the Thesis submitted for assessment and defence, exclusively contains the results of my own work assisted by my supervisor. Further to it, it is also stated that all other results taken from the technical literature or other sources are clearly identified and referred to according to copyright (footnotes/references are chapter and verse, and placed appropriately).
I accept that the scientific results presented in my Thesis can be utilised by the Department of the supervisor for further research or teaching purposes.

Budapest, on the 13th of December, 2019

_____
(Signature)

FOR YOUR INFORMATION

The submitted Thesis in written and in electronic format can be found in the Library of the Department of Fluid Mechanics at the Budapest University of Technology and Economics. Address: H-1111 Budapest, Bertalan L. 4-6. „Ae" building of the BME.

ACKNOWLEDGEMENT

The research reported in this current investigation has been supported by the János Bolyai Research Scholarship of the Hungarian Academy of Sciences, by the ÚNKP-19-3 New National Excellence Program of the Ministry of Human Capacities, by the Higher Education Excellence Program of the Ministry of Human Capacities in the

frame of Water science & Disaster Prevention research area of Budapest University of Technology and Economics (BME FIKP-VÍZ), and by the National Research, Development and Innovation Fund (TUDFO/51757/2019-ITM, Thematic Excellence Program).

I would like to express my gratefulness to our supervisors **Dr. Csaba Horváth** and **Dr. Josh Davidson** for giving me support and guidance in this topic.

ABSTRACT

As the composition of the energy mix shifts thoughout the years towards sustainable energy generation, the interest in various renewable energy sources has skyrocketed. This includes the Wave Energy Converters (WEC), which have been considered one of the most promising sources. Wave Energy is a distinguished opportunity for coastal countries. The Oscillating Water Column (OWC) is the most researched WEC, because of its simplicity and capability of long-term operation.

The greatest tool in the development and optimisation of OWC technology is Computational Fluid Dynamics (CFD). Using CFD simulations various geometries and approaches can be studied and compared cost-effectively, as no real-life model is needed for these experiments. The biggest drawback in CFD simulations is the need to compromise between accuracy and computational time. Finer meshes can lengthen the computational time exponentially with only slightly more accurate results. Therefore the main goal in setting up these CFD models is to find a balance between accuracy and time.

In the present work the various developments in OWC technology are summarized, mainly in CFD applications. This is followed by a examination and comparison of various mesh approaches of the OWC chamber, highlighting the shortcomings of each and making suggestions for further improvements. The numerical simulations were conducted using commercial CFD-based ANSYS Fluent 19.1 software. The output of the CFD modeling effort performed by our team is to be submitted to the International Energy Agency's Ocean Energy Systems "Task 10 - Wave Energy Converter (WEC) modelling verification and validation project”. The project investigates the possibility to include simulations that will support the development of standards under the International Electrotechnical Commission (IEC). The particular oscillating water column (OWC) test case represents model scale testing performed by Korea Research Institute of Ship & Ocean Engineering (KRISO).

KIVONAT

Ahogy az energia mix az évek során a fenntartható energia fejlesztés felé változik, megnövekedett az érdeklődés egyes megújuló energiaforrások iránt. Ezek közé tartozik a Hullám Energia Átalakítók (Wave Energy Converter – WEC), melyet a legigéretesebbek közé sorolnak. Az Oszcilláló-víz-oszlop (Oscillating Water Column – OWC) a legtöbbet kutatott WEC közé tartozik, egyszerűsége és hosszú távú működési képessége miatt.

A legfontosabb eszköze az OWC-k fejlesztésének és optimalizálásának a numerikus áramlástan (Computational Fluid Dynamics - CFD). A CFD szimulációk segítségével költséghatékonyan lehet különböző geometriákat vizsgálni és összehasonlítani, hiszen nem szükséges drága laboratóriumi modellek építése. A legnagyobb hátránya a CFD szimulációknak a pontosság és a szimuláció futási ideje (számítási igény) közti kapcsolat. A finomabb háló exponenciálisan növeli a számítási igényt, viszont a pontosság növekedése messze nem ilyen jelentős. Kijelenthető, hogy az egyik legfontosabb cél a szimulációs modell felállításánál, hogy az adott problémának megfelelően, a pontosság és a számítási igény közötti egyensúlyt megtaláljuk.

E dolgozat az OWC fejlesztéseit összegzi az évek során. Végezetül részletezi az OWC tartály különböző hálózási megközelítéseinek vizsgálatát és összehasonlítását, kiemelve a hátrányosságaikat és a további fejlődési lehetőségeket. A numerikus szimulációk kereskedelmi CFD szoftverrel lettek elvégezve. A szimulációs projektünk célja az International Energy Agency's Ocean Energy Systems által meghirdetett "Task 10 - Wave Energy Converter (WEC) modelling verification and validation project” elnevezésű kutatásba való bekerülés. A projekt vizsgálja annak a lehetőségét, hogy bevonja azon szimulációkat, melyek az International Electrotechnical Commission (IEC) előírásainak fejlesztését támogatják. A kiírt OWC egy, a Korea Research Institute of Ship & Ocean Engineering (KRISO) által definiált és elvégzett modell kísérlet.

CONTENTS

1. INTRODUCTION

The Oscillating Water Column (OWC) is a type of wave energy converter (WEC) which consists of a fixed or an oscillating hollow structure, open to the sea below the water surface, which traps air above the inner free surface. The waves periodically compress and decompress the trapped air which forces it to flow through a turbine coupled to a generator. The advantages of an OWC are that the only moving part of the energy generating mechanism is the rotor of the turbine and it is located above the water level, so higher rotational speeds and greater lifetime can be achieved. Furthermore the OWCs can be built close to the sea shore for easy access to the power grid and for maintenance.

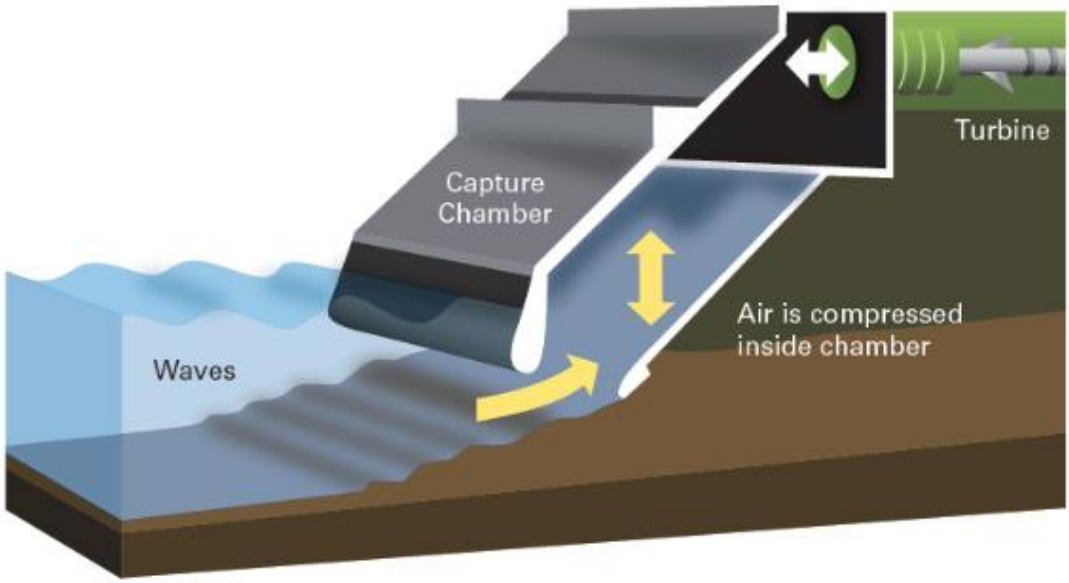

Figure 1.: The schematic of an OWC [23]

2. LITERATURE SURVEY

2.1. OWC technology

The first device, what was only later considered as an OWC, was a navigation buoy equipped with a unidirectional turbine [1,2]. The airflow was redirected with a system of non-return valves. This system, as later studies have shown, is impractical for larger structures and inefficient, as the non-return valves response time is too long [3].

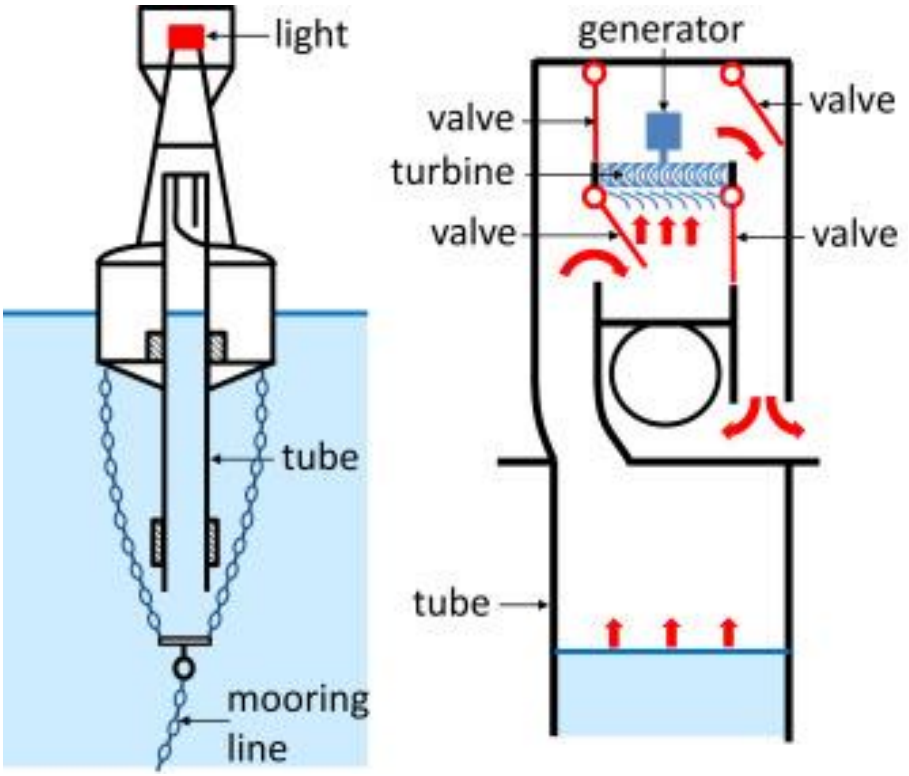

Figure 2.: Schematic of Masuda's navigation buoy [2]

As a result, self-rectifying turbines were considered. This kind of turbine is designed to rotate in one direction regardless of the incident flow direction. The most researched and used self-rectifying turbine is the Wells turbine, due to its simple geometry and high efficiency.

2.1.1. Wells turbine

The Wells turbine is a low-pressure self-rectifying turbine. It has symmetrical airfoil blades with its plane of symmetry is perpendicular to the airstream.

Other advantages of this design are the higher energy storage capability and higher rotor blades speeds, but the later causes bigger aerodynamic noises. The problems of this design are the poor self-starting capability, narrow operating flow range, high exit losses, and sudden efficiency drop caused by stalling. Various improvements were studied to overcome these design's shortcomings. Guide vanes were proposed to minimize swirling exit flow losses, and widen the operating range before stalling. For the later, self-pitch-controlled blades were also studied. Biplane and contra-rotating Wells turbines were proposed for these problems [4].

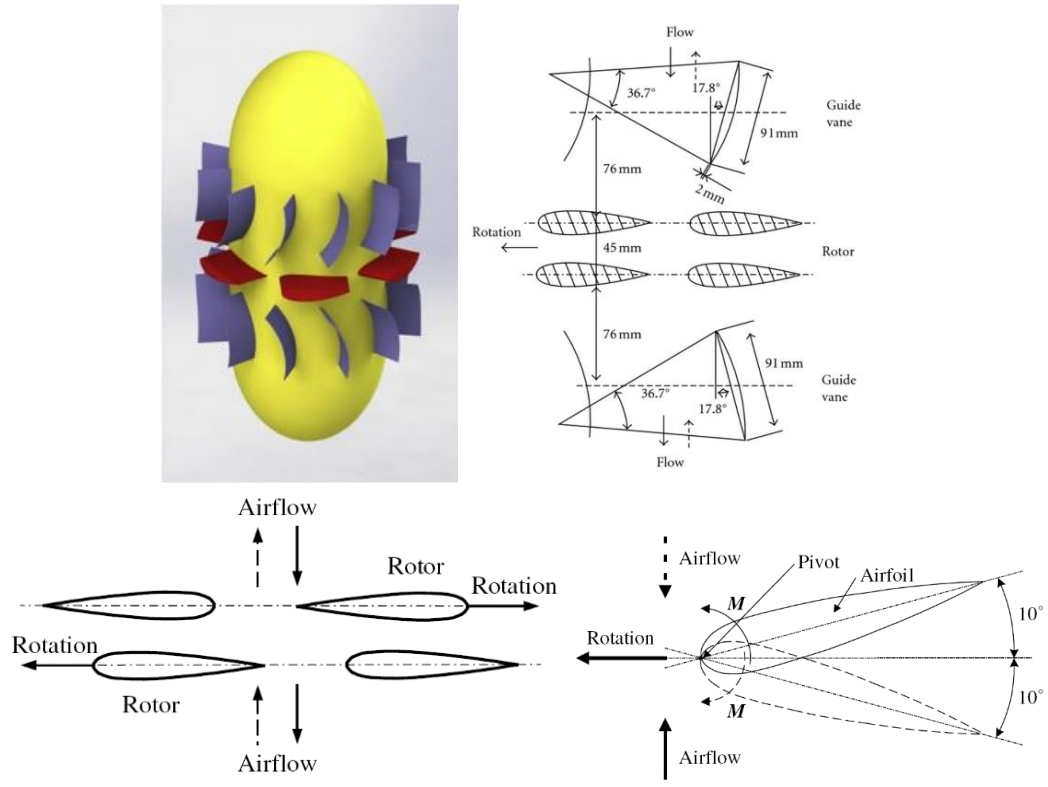

Figure 3.: 3D model of Wells turbine with guide vanes, Schematic of Biplane Wells turbine with guide vanes, Contra-rotating Wells turbine, self-pitch-controlled Wells turbine respectively [2]

2.1.2. Impulse turbine

The other widely studied turbine design is the impulse turbine shown on Figure 4. The geometry of the rotor blades is a modified symmetrical version of an impulse steam turbine. The exit angle of the blades approximately equals the exit flow angle. This design has a wider operating flow range, but a lower peak efficiency due to the excessive incidence flow angle at the entry of the second row of guide vanes. [2].

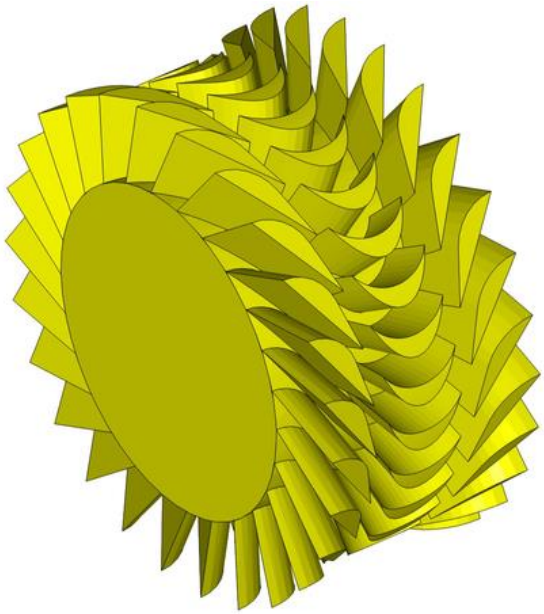

Figure 4.: 3D model of impulse turbine [2]

2.1.3. Other types of self-rectifying turbines

Other experimental turbines were also proposed. The HydroAir turbine, shown on Figure 5., is a modified impulse turbine. At the inlet and outlet guide vanes are implemented, which gives a swirl motion to the flow. The air accelerates as it travels through a narrowing duct towards the turbine, and decelerates in the expanding duct. This design promises a wider operating range and lower noise [5].

Figure 5.: The HydroAir turbine [5]

The Dennis-Auld turbine is a controlled variable-pitch Wells turbine, where the setting angle is between $20° < \gamma < 160°$, resulting in a higher, 65% efficiency [2].

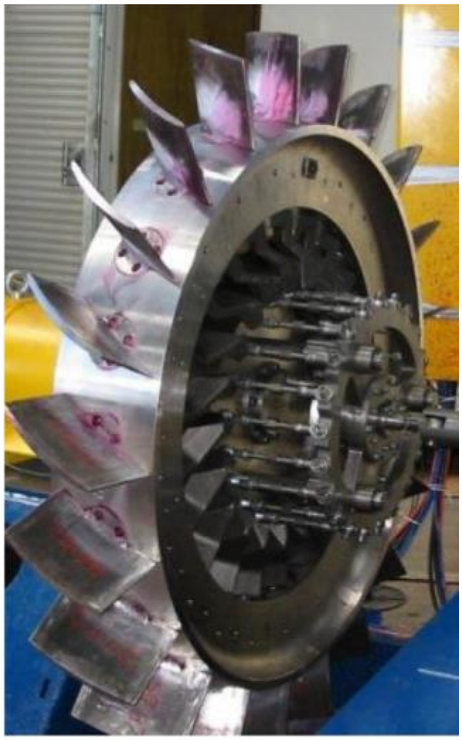

Figure 6.: Dennis-Auld turbine [2]

The self-rectifying radial turbine consists of a pair of guide vanes mounted on the periphery of the rotor. The rotor slides inside the guide vanes moved by gravity and aerodynamic forces [2].

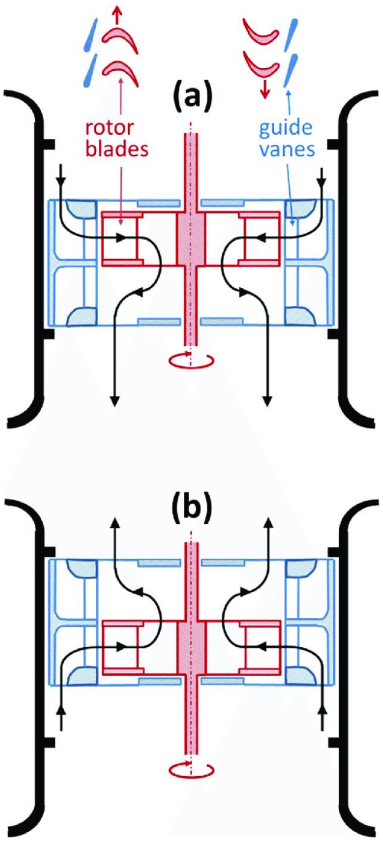

Figure 7.: Self-recifying radial turbine [2]

2.2. CFD simulation methods

Computational Fluid Dynamics (CFD) is a branch of the fluid mechanics that, with the help of computers, provides quantitive predictions of fluid flow based on conservation laws governing the fluid motion [6]. It became an essential tool for designing and optimizing turbomachinery. To reduce the computational costs and maintain precision of the Navier-Stokes equations, the Reynolds-averaged Navier-Stokes (RANS) equations were proposed by Osborne Reynolds in 1895 [7]. In this paper the governing equations are:

Continuity equations:

$$\frac{\partial \rho}{\partial t} + \frac{\partial}{\partial x_i}(\rho u_i) + \frac{\partial}{\partial x_j}(\rho u_j) + \frac{\partial}{\partial x_k}(\rho u_k) = 0$$

RANS equations:

$$\frac{\partial}{\partial t}(\rho u_i) + \frac{\partial}{\partial x_j}(\rho u_i u_j) =$$

$$= -\frac{\partial p}{\partial x_i} + \frac{\partial}{\partial x_j}\left[\mu\left(\frac{\partial u_i}{\partial x_j} + \frac{\partial u_j}{\partial x_i} - \frac{2}{3}\delta_{ij}\frac{\partial u_j}{\partial x_i}\right)\right] + \frac{\partial}{\partial x_j}(-\rho\overline{u'_i u'_j})$$

$$\frac{\partial}{\partial t}(\rho u_j) + \frac{\partial}{\partial x_k}(\rho u_j u_k) =$$

$$= -\frac{\partial p}{\partial x_j} + \frac{\partial}{\partial x_k}\left[\mu\left(\frac{\partial u_j}{\partial x_k} + \frac{\partial u_k}{\partial x_j} - \frac{2}{3}\delta_{jk}\frac{\partial u_k}{\partial x_j}\right)\right] + \frac{\partial}{\partial x_k}(-\rho\overline{u'_j u'_k})$$

$$\frac{\partial}{\partial t}(\rho u_k) + \frac{\partial}{\partial x_j}(\rho u_k u_i) =$$

$$= -\frac{\partial p}{\partial x_k} + \frac{\partial}{\partial x_i}\left[\mu\left(\frac{\partial u_k}{\partial x_i} + \frac{\partial u_i}{\partial x_k} - \frac{2}{3}\delta_{ki}\frac{\partial u_i}{\partial x_k}\right)\right] + \frac{\partial}{\partial x_i}(-\rho\overline{u'_k u'_i})$$

where ρ is the air density, p is the air pressure, x_i, x_j, x_k are the coordinates, u_i, u_j, u_k are the velocities in respect of the coordinates, and δ_{ij} is the Kronecker delta. The last term $\frac{\partial}{\partial x_j}(-\rho\overline{u'_i u'_j})$ is referred to the Reynolds stresses, and represents the effects of turbulence.

To close these equations and model the turbulence term, the Boussinesq approximation was used.

2.2.1. Turbulence models

To close the RANS equations we need to model the Reynolds stress terms as a function of the mean flow. Various turbulence models are used to solve these equations [8]:

2.2.1.1. Spalart-Allmaras (S-A) model:

The Spalart-Allmaras model is a one-equation model that solves a modelled transport equation for kinematic eddy viscosity. It is designed for wall-bounded flows and gives good results for boundary layers in adverse pressure gradients [8].

2.2.1.2. Standard k- ε model:

The standard k-ε model is a semi-empirical model based on model transport equations for the *k* turbulence kinetic energy and its ε dissipation rate.

$$k = \frac{\overline{u'^2 + v'^2 + w'^2}}{2} \left[\frac{m^2}{s^2}\right] \qquad \varepsilon = \frac{dk}{dt} \left[\frac{m^2}{s^3}\right]$$

, where the u', v' and w' are the fluctuating velocities in respect of the coordinates.

In this model, the assumption is that the flow is fully turbulent and the effects of molecular viscosity are negligible [8].

2.2.1.3. Renormalization Group (RNG) k-e model:

The RNG k-ε turbulence model uses a mathematical technique called renormalization group method to overcome the semi-empirical nature of the k-ε model. This model has higher accuracy for rapidly strained and swirling flows and accounts for low Reynolds numbers effects [8].

2.2.1.4. Realizable k-ε model:

The realizable k-ε model combines the Boussinesq approximation and the eddy viscosity equations. This model more accurately predicts the spreading rate of planar and round jets. Furthermore, it provides better performance for flows involving rotation or for boundary layers with adverse pressure gradients, separation and recirculation [8].

2.2.1.5. Standard k-ω model:

The standard k-ω model is an empirical model based on the turbulence kinetic energy and the specific dissipation rate ω, which can be thought of as the ratio of ε to k. This model gives accurate results for far wakes, mixing layers and various jets. Therefore, the k-ω model regarded as a suitable model for wall-bounded flows and free shear flows [8].

2.2.1.6. Shear-stress-transport (SST) k-ω model:

Combines the standard k-ω model in near-wall regions, and the transformed k-ε model in far-field regions. This model is more accurate and reliable for different types of flows the standard k-ω model [8].

2.3. CFD for OWC chamber applications

Sarmento and Falcao [9] used linear wave theory to describe the incoming waves. They found that air compressibility can significantly affect the performance of full-scale devices. First, the free surface was assumed to be a piston-like horizontal flat surface, which was later changed to a warped free surface and spatially uniform air pressure. Because of the nonlinearity of the pressure oscillations, time-domain analysis is used free surface equations instead of frequency domain analysis. But due to complexity, this analytical method was neglected in CFD applications.

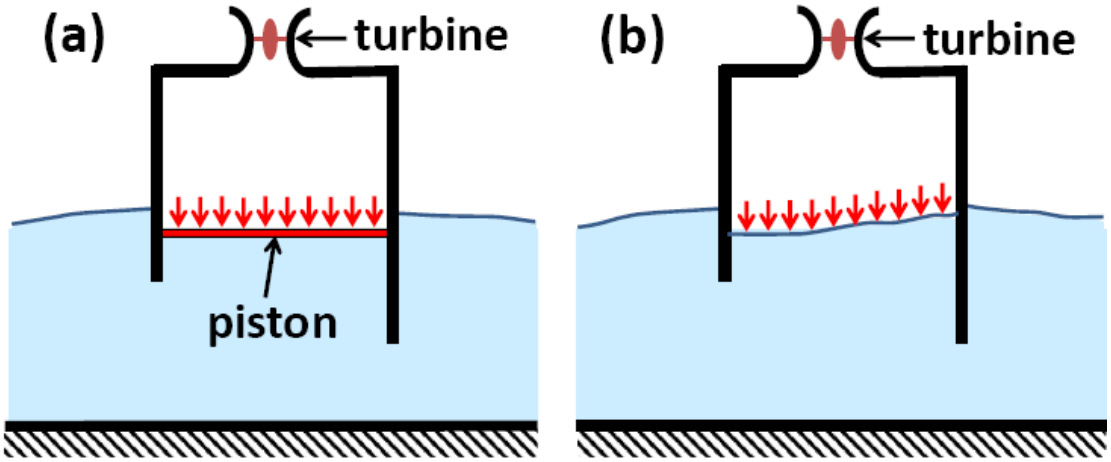

Figure 8.: Schematic representation of OWC modelling [2]

They also found that the spring-like effect of the air compressibility inside the chamber can be disregarded, as it is more prevalent between the turbine and the chamber. This compressibility effect introduces a phase difference between the flow rate inside the chamber and the turbine.

2.4. CFD for OWC turbo machinery applications

As the approaches for modelling the OWC chambers and turbines are vastly different, including the time-scale difference and the mesh density, studied separately.

2.4.1. Computational domains and reference frames

The first numerical studies in the self-rectifying turbines were conducted on the Wells turbine [10]. To minimize the computational load, the computational domain was divided to a single rotor blade with periodic boundaries. In the early stages, a single rotating frame (SRF) were used. Further studies found that, when the rotational speed is constant, a quasi-steady assumption can be made. [11]

As the guide vanes are employed for the Wells turbine, a mixing plane (MP) was used between sub-domains of the CFD model. This solved the problem of the number difference between the guide vanes and blades [12]. Some studies used the multiple reference frame (MRF) approach, but this does not consider the relative motions between adjacent zones. Instead the moving zone is fixed and an instantaneous flow field is calculated.

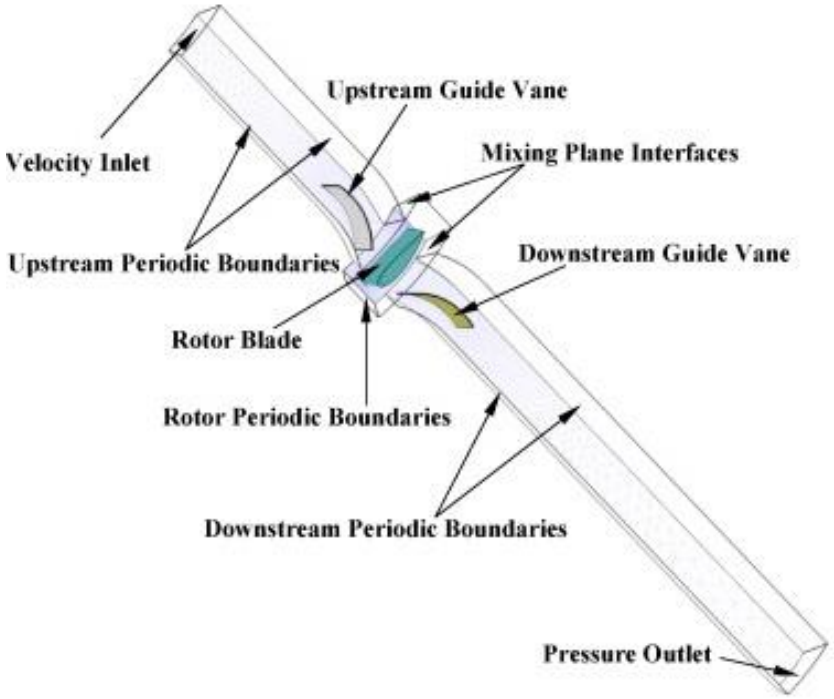

Figure 9.: Schematic of a Wells turbine computational domains

Using a sliding mesh (SM) model the stationary and rotational sub-domains remain connected, ensuring an accurate flux exchange and a faster computational convergence [13].

In these studies, the most used turbulence models are the k-ε, Realizable k-ε and the SST k-ω. Further explanations were not included.

2.4.2. Improvements of the Wells turbine

For the improvement on the geometry of the Wells turbine, including the blade geometry, solidity, hub-to-tip ratio, sweep angle and tip clearance, various studies were conducted. The most researched blade geometries are the NACA0015, NACA0018 and the NACA0020. Multiple studies found that increasing the blade thickness, for example from NACA0015 to NACA0020, increases the efficiency of the turbine, and widens the operational range [14, 15]. One study used an OPAL optimizer to calculate an optimal shape for the blade cross-section [16].

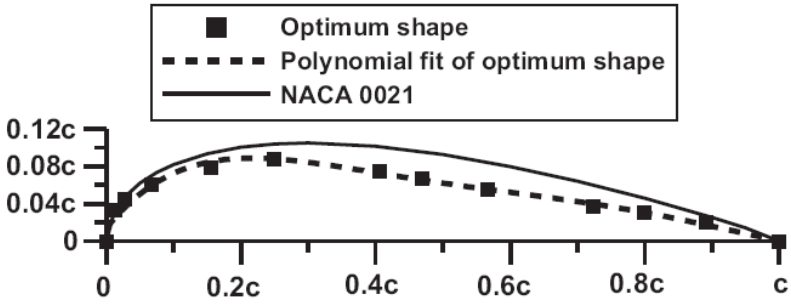

Figure 10.: Comparison between the NACA0021 , the polynomial fit of the optimal shape and the optimal shape by splines [16]

Watterson and Raghuanathan in 1998 [17] found that increasing the blade solidity strengthens the interaction between the adjacent blades and moves the stall point to higher flow coefficient region. The blade solidity is defined as the ratio of blade length to pitch. These results are confirmed by other studies [15].

In 2016 Halder et al. [18] studied the effects of the blade sweep. They found that a blade with backward swept mid-section and forward swept tip-section has a smaller separation layer, and a blade with a forward sweep angle has a higher torque.

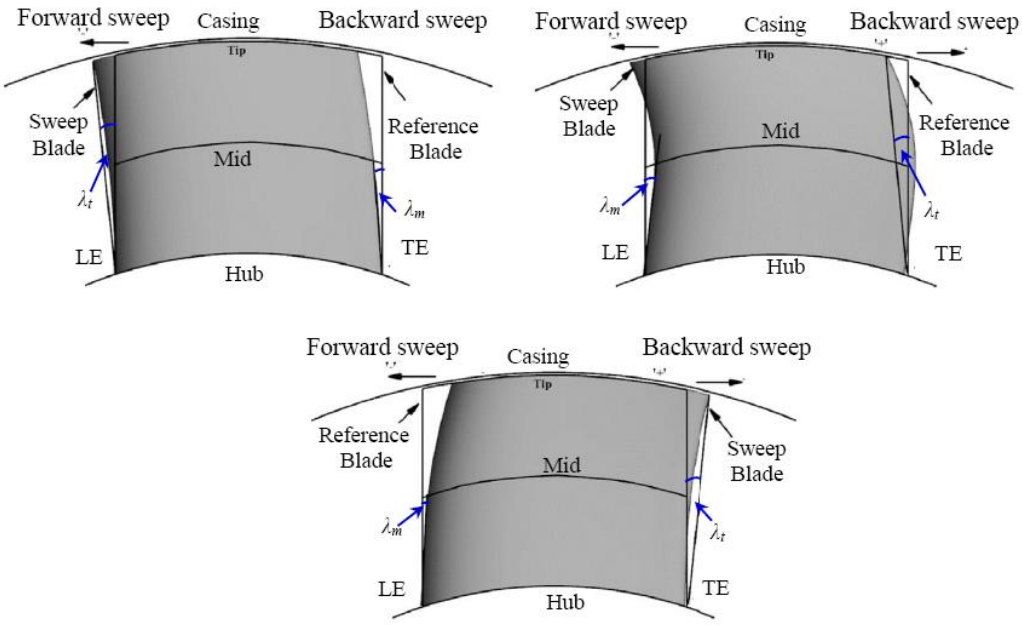

Figure 11.: Schematic of the different blade sweeps

Torresi et al. [19] found in 2004 that the tip clearance reduces the pressure drop at the blade tip, thus decreases the hysteretic behaviour of the turbine and reduces the torque coefficient as well. Taha et al. [20] investigation confirmed this finding.

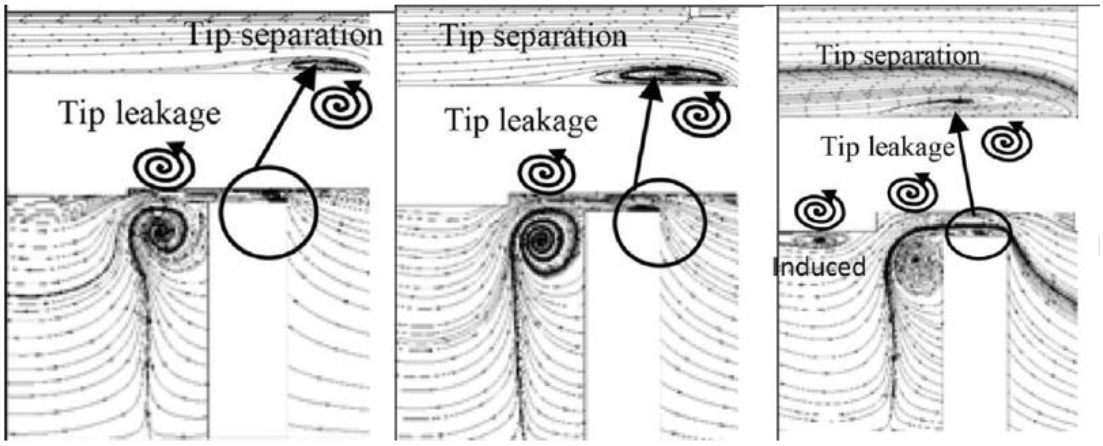

Figure 12.: Representation of the tip leakage vortices [19]

In 2015 Cui and Hyun [21] improved the tip clearance design by introducing a penetrating endplate and ringplate tip clearance, increasing the efficiency of the turbine.

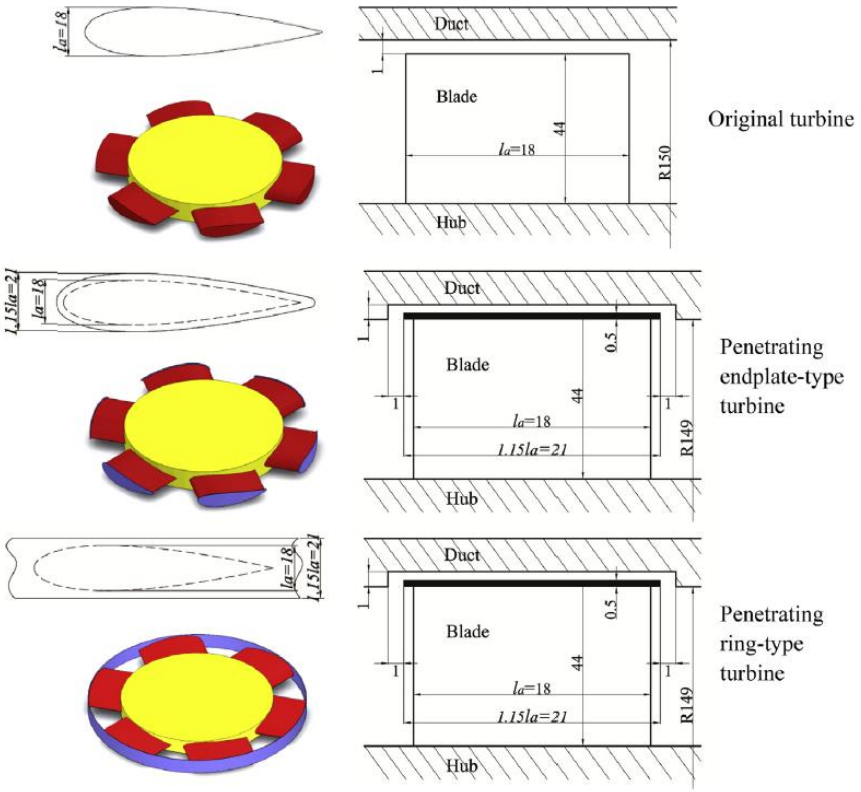

Figure 13.: Geometric comparison between the different tip leakage geometries [21]

3. OWC CHAMBER MESHING

In this Section, the meshing of the chamber is described. Section 3.1 details the geometry of the chamber and duct, Section 3.2 presents the two-dimensional case study and Section 3.3 presents the three-dimensional summary.

3.1. Chamber geometry

The experimental model of the OES Task 10 is shown on Figure 12. Task 10 is a verification and validation project for numerical models for wave energy converters. The project is run by the International Energy Agency (IEA) – Ocean Energy Systems (OES). The OWC chamber is placed on the bottom of the basin with 3.2 m of depth. The interior length of the chamber is 1.25 m, and the skirt extends vertically below the mean sea level. A duct with a diameter of 0.2 m and a height of 0.5 m is located at the top of the OWC chamber. At the center of the duct, an orifice was applied with a thickness of 0.003 m. [22]

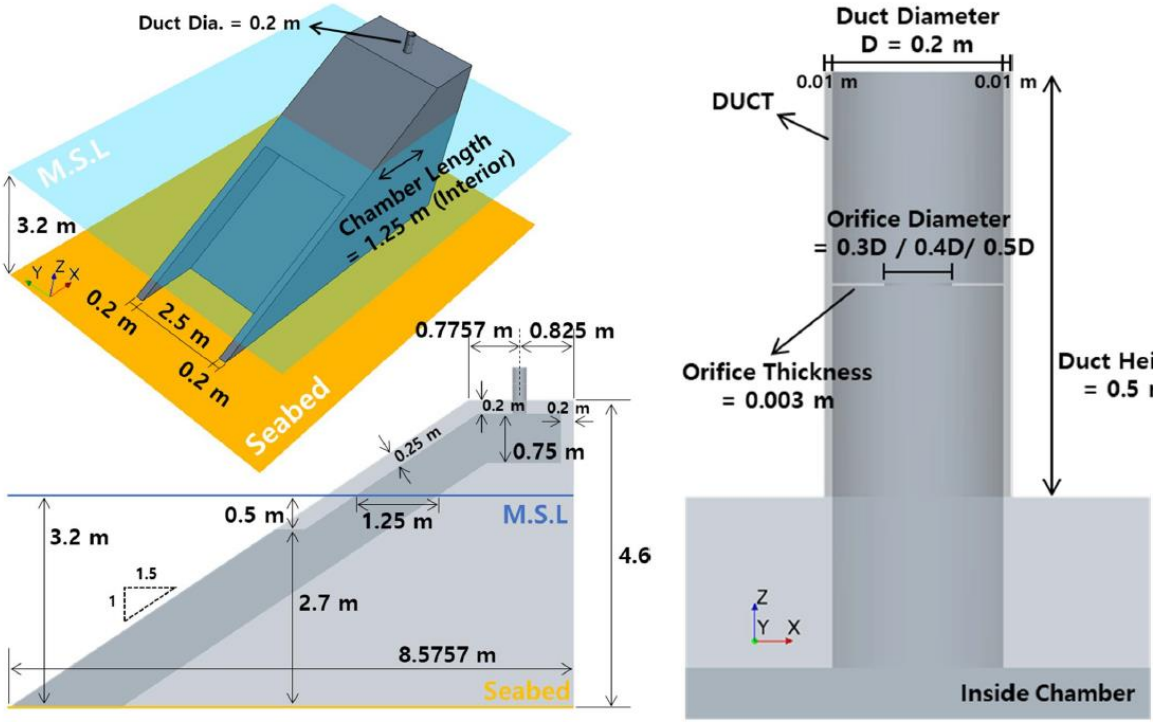

Figure 14: The dimensions of the experimental OWC chamber and duct [22]

3.2. Two dimensional Analysis of the OWC Chamber.

In this Section the construction of a two dimensional model and the mesh independence study is described. The advantage of a 2D simulation over a 3D one is the faster computational time, because of the fewer cells and simplification of the numerical equations. It allows to make quick comparisons between various meshing and modelling methods, including differences between mesh densities, the importance of the boundary layer on the chamber wall, and the difference between compressible and incompressible flow.

3.2.1. Geometry of the model

The geometry of the model is a vertical cross-section of the experimental one at the center of the duct with a 2 m high outer region above the exit of the duct. The bottom of the model is the mean sea level. Instead of a waving water surface, the bottom of the chamber is described as a horizontal wall with a sinusoidal motion. The main difference between the waving water and the moving wall is the water surface, from the experimental data shown on Figure 15., moves on the back of the chamber slower and the front of the chamber faster than the horizontal surface.

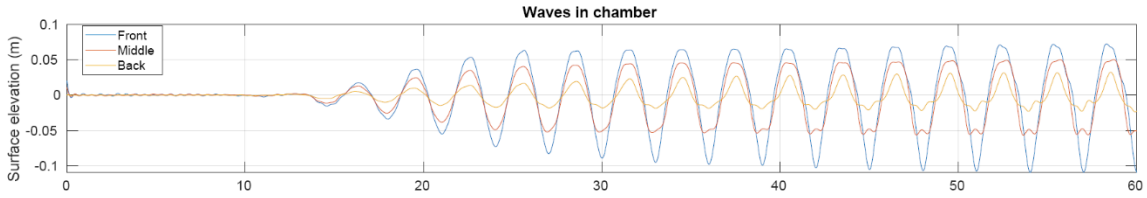

Figure 15.: The water surface elevation inside the OWC chamber

The movement of the wall was described with a User Defined Function (UDF) with the wave height H = 0.089 [m] and period T = 3.5 [m]. Around the moving wall, the mesh was corrected with layering. The layering algorithm collapses two neighbouring cells or divides one in two if the cell reaches a certain height ratio.

3.2.2. Construction of the mesh

In the mesh study, 4 meshes were compared. In the first case, the bottom of the chamber 25 cells were used and 106 along its length. On the width of the duct 26 cells and height 32 cells were used. The outer region was divided to 63 cells along its width, and 28 on its height

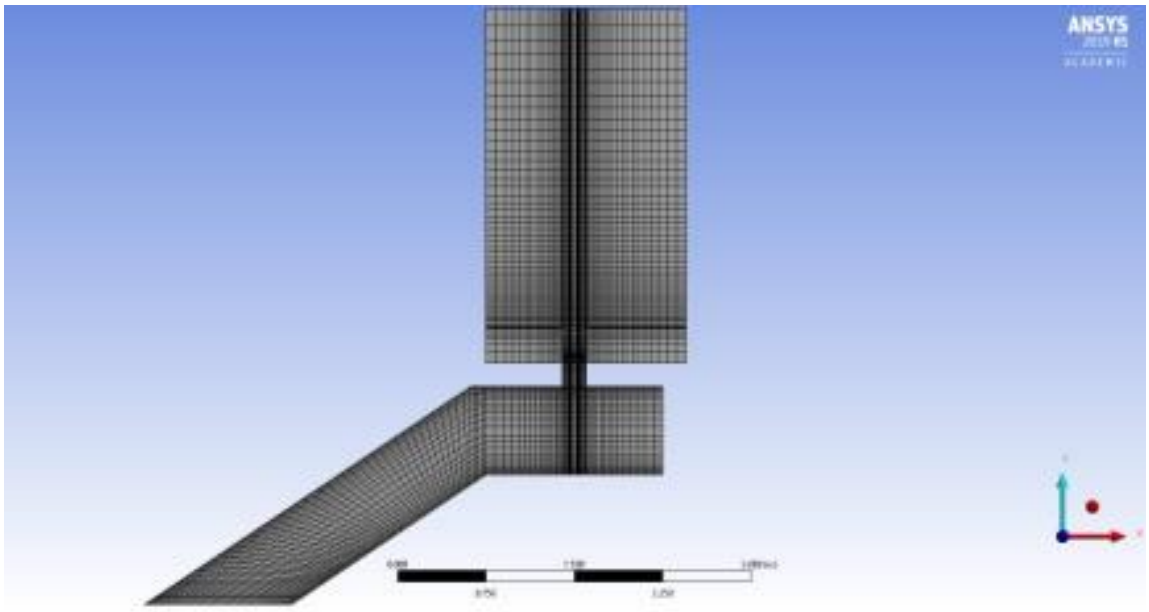

Figure 16.: The mesh in the first case

These number of divisions were multiplied by 2, 3 and 4 to construct the other cases. The exact values are shown in Table 1.

Number of the case	Number of cells/ width of the chamber	Number of cells/ height of the chamber	Number of cells/ width of the duct	Number of cells / height of the duct	Number of cells/ width of the outer region	Number of cells/ height of the outer region	Cell number of the case
1.	25	106	26	32	63	68	6880
2.	50	207	50	64	152	115	33030
3.	75	290	70	93	178	170	57390
4.	100	315	100	124	244	230	107460

Table 1.: The number of cells on the geometry

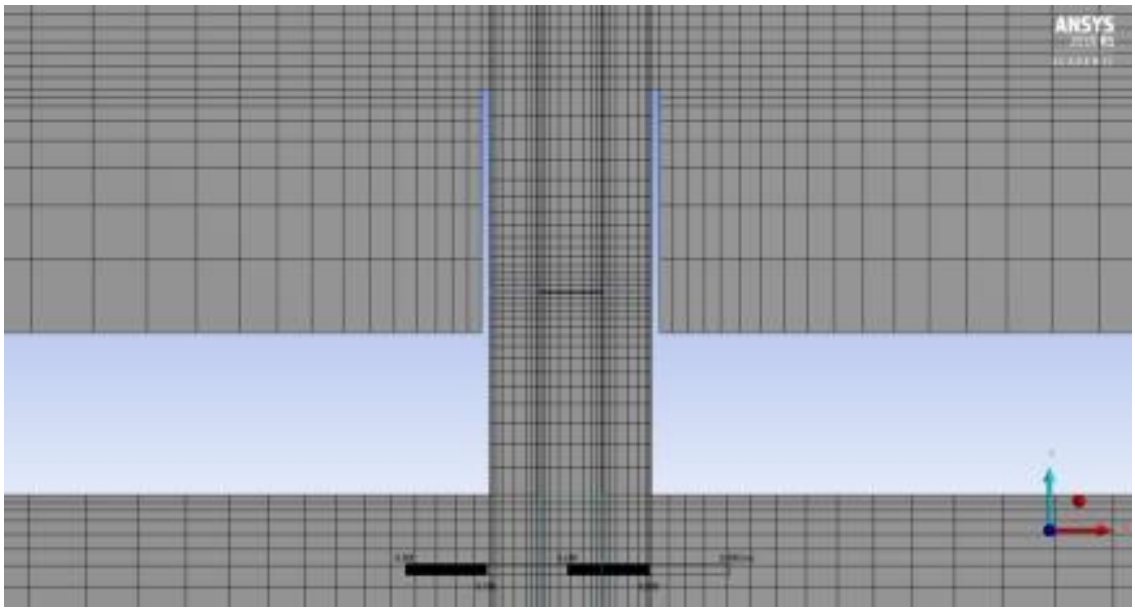

Figure 17.: Mesh in the duct in Case 1.

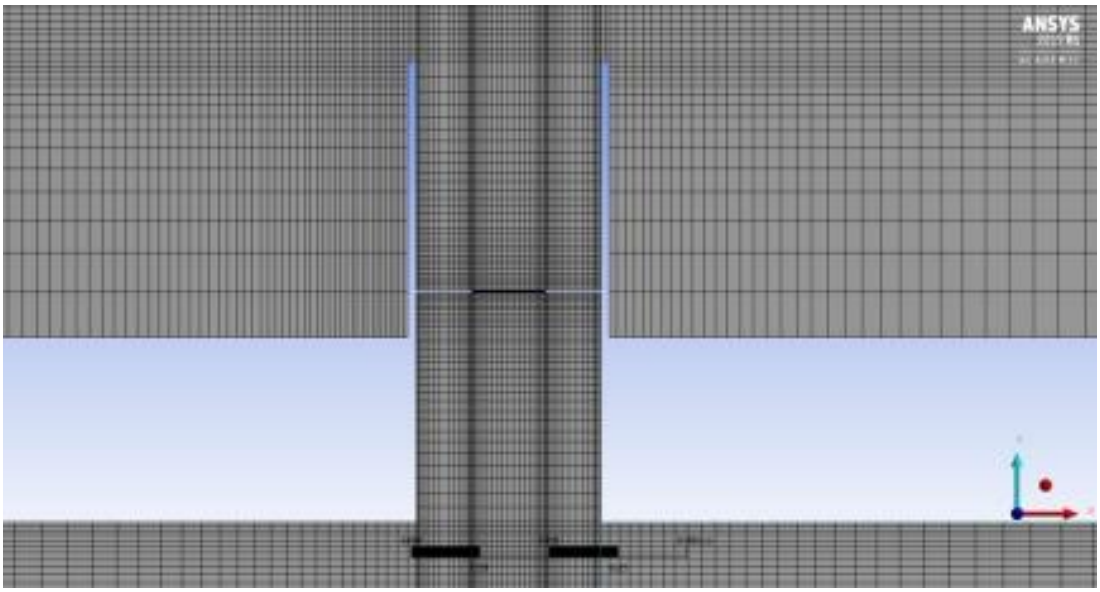

Figure 18.: Mesh in the duct in Case 2.

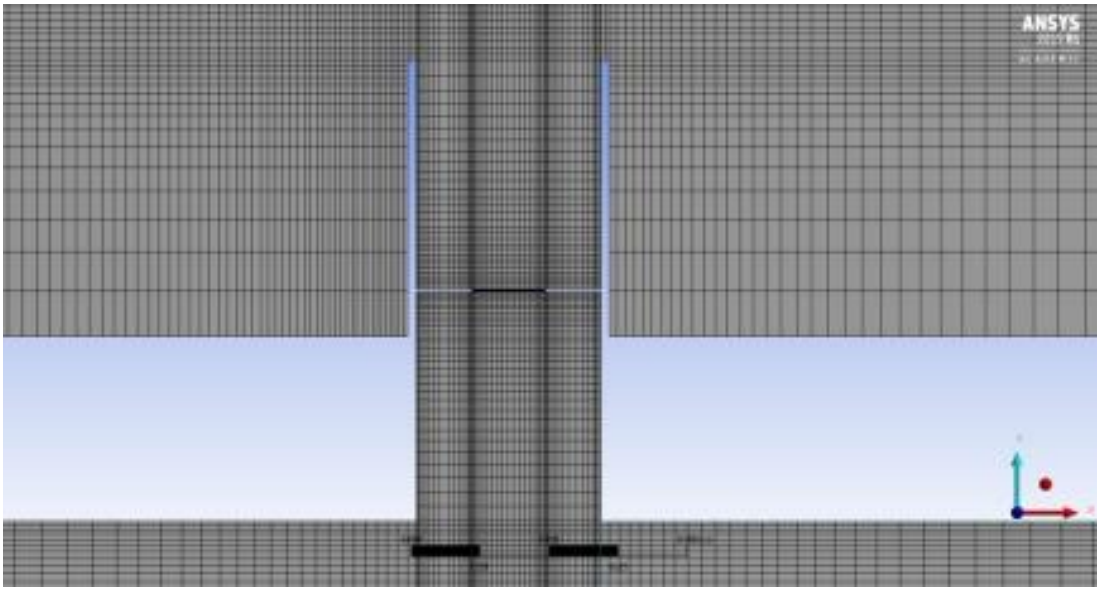

Figure 19.: Mesh in the duct in Case 3.

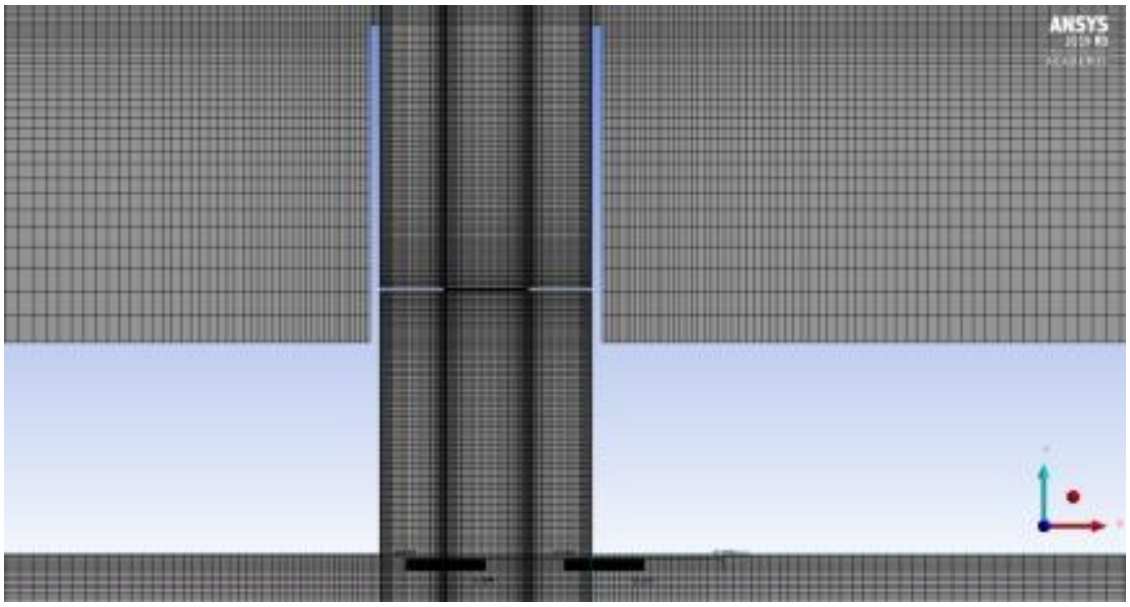

Figure 20.: Mesh in the duct in Case 4.

3.2.3. Temporal resolution.

The simulation of the chamber was first done in a CFL-based calculation. This method was discarded due to its inaccurate results, which are shown on Figure 21-23.

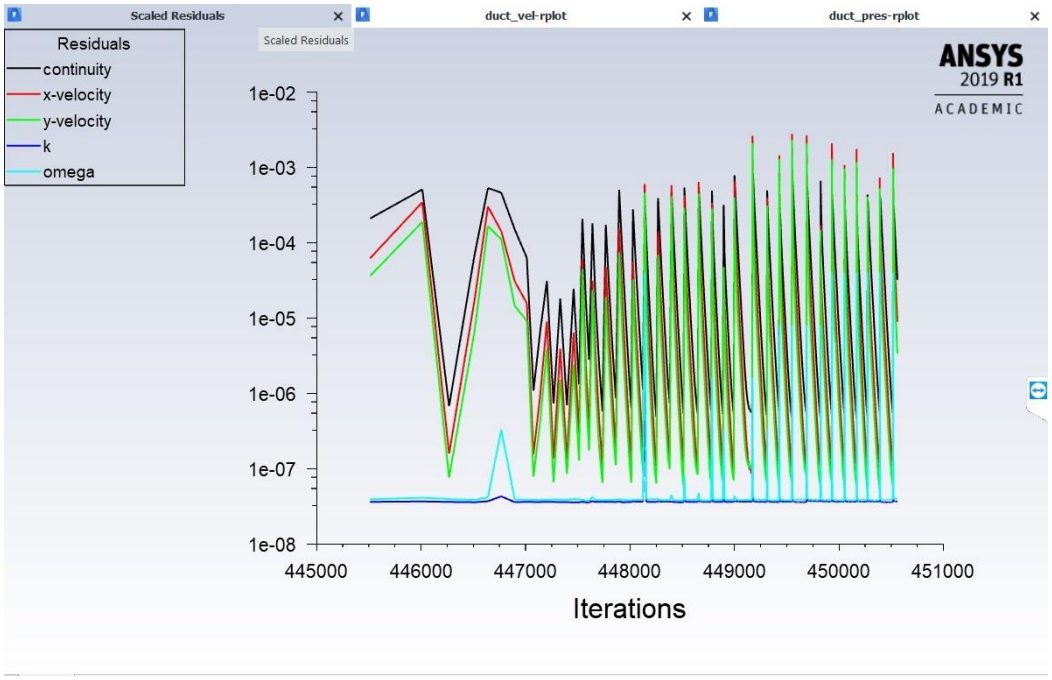

Figure 21.: The graph of the residuals in the CFL-based calculation

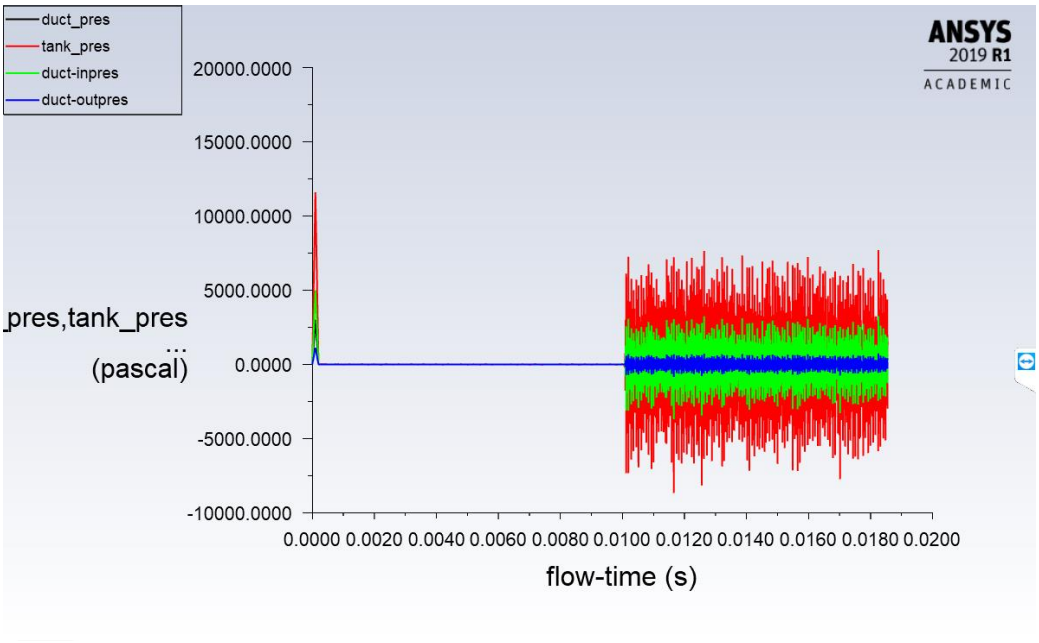

Figure 22.: Graph of static pressure values in the chamber (red), inner (green) and outer (blue) exit of the duct and at the orifice (grey)

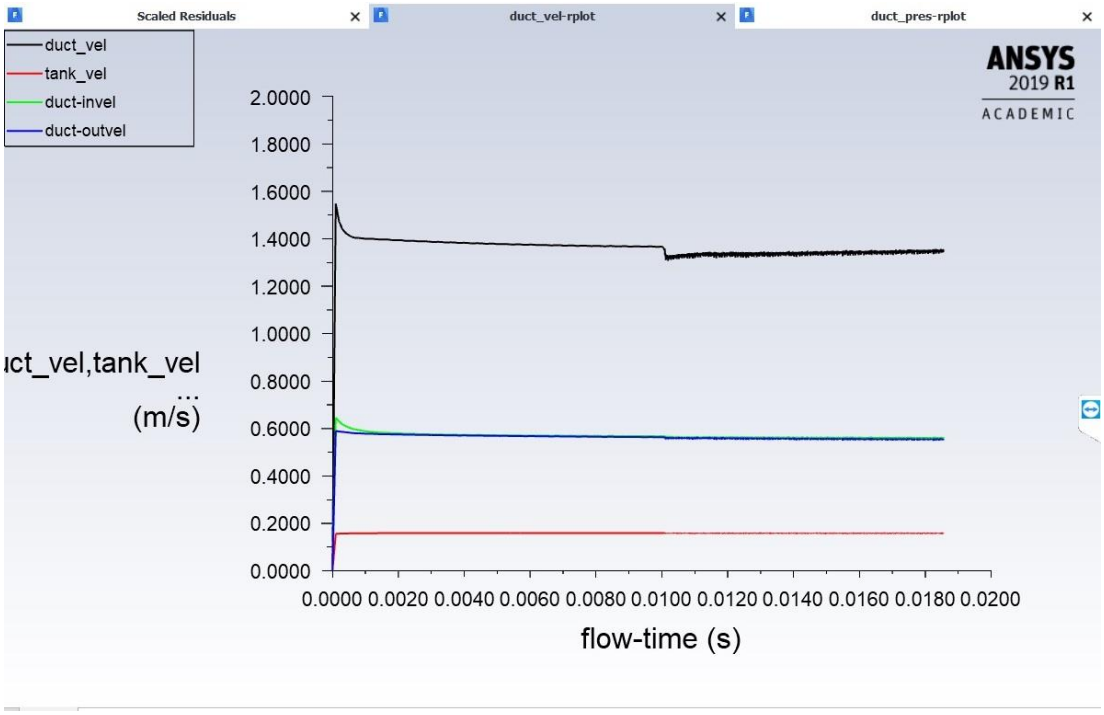

Figure 23.: Graph of the velocity magnitude inside the chamber (red), inner (green) and outer (blue) exit of the duct and at the orifice (black)

These results may be caused by the motion of the wall or from the structure of the mesh. Because of this, it was necessary to decide the length of a fixed time step, choosing between the temporal resolution and computational time.

A comparison study was done, using two time steps, 0.01 [s] and 0.001 [s]. The results were calculated on the Case 2. mesh, the results of the velocity magnitude at the orifice are shown on Figure 24.

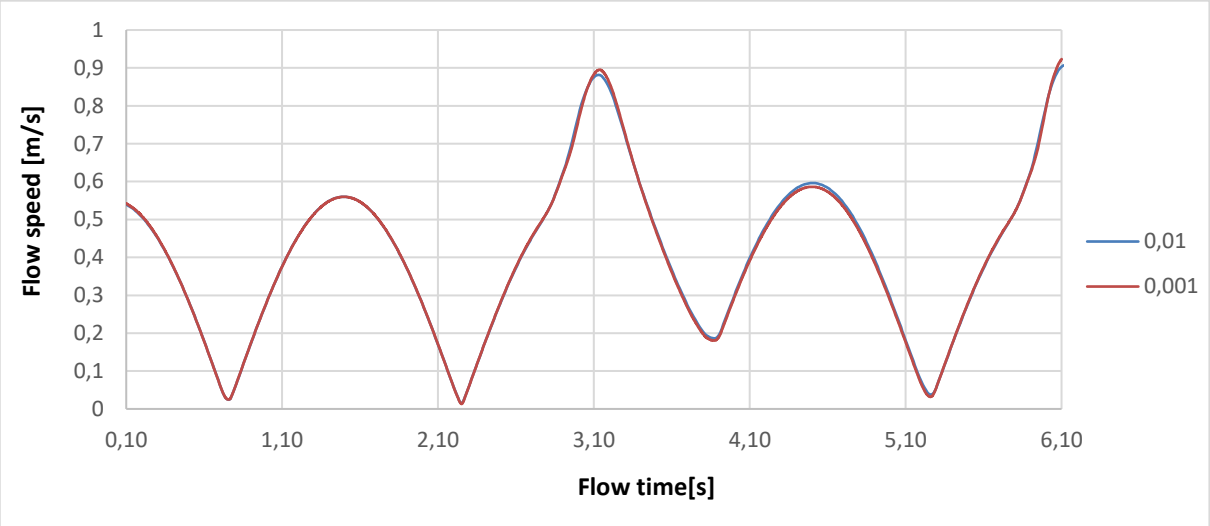

Figure 24.: The comparison between the flow speeds in different time steps

As it is shown on the graph, the differences are negligible. The difference is 0.001 [m/s] at 3.75 [s] and 0.048 [m/s] at 4.5 [s].

3.2.4. Mesh convergence study

In this section, a mesh convergence study is done on the four cases. Compared results are the static pressures and flow speeds on the inner and outer exit of the duct and at the orifice, and the volumetric flow rate through the duct. The orifice was chosen as in the experimental measurements were done around it. The exits of the duct were measured for using these as boundary condition values for future turbine studies.

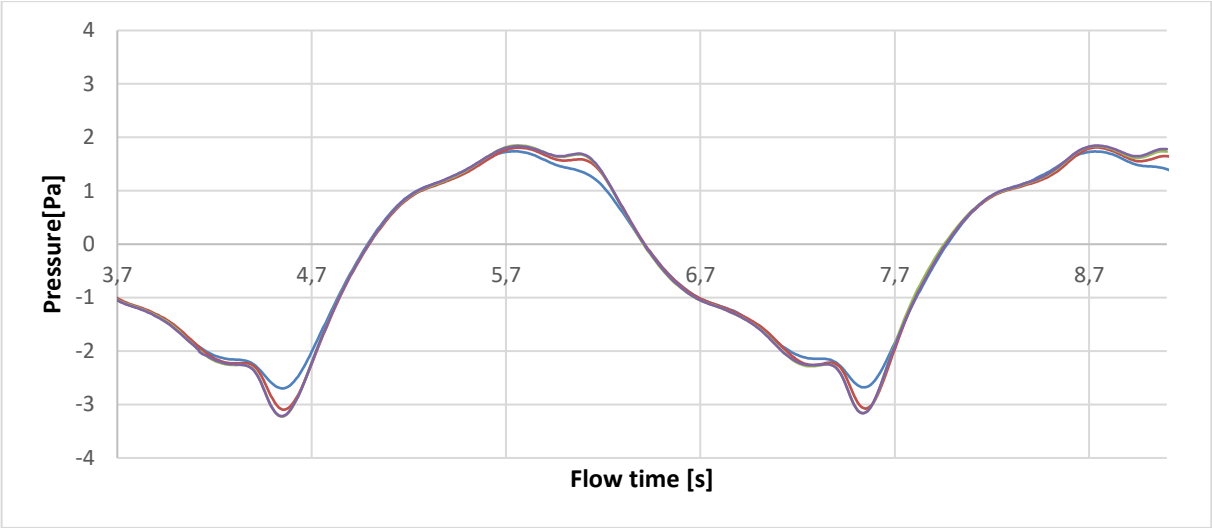

Figure 25.: Pressure values at the inner exit of the duct (blue: Case 1, red: Case 2, yellow: Case 3, purple: Case 4)

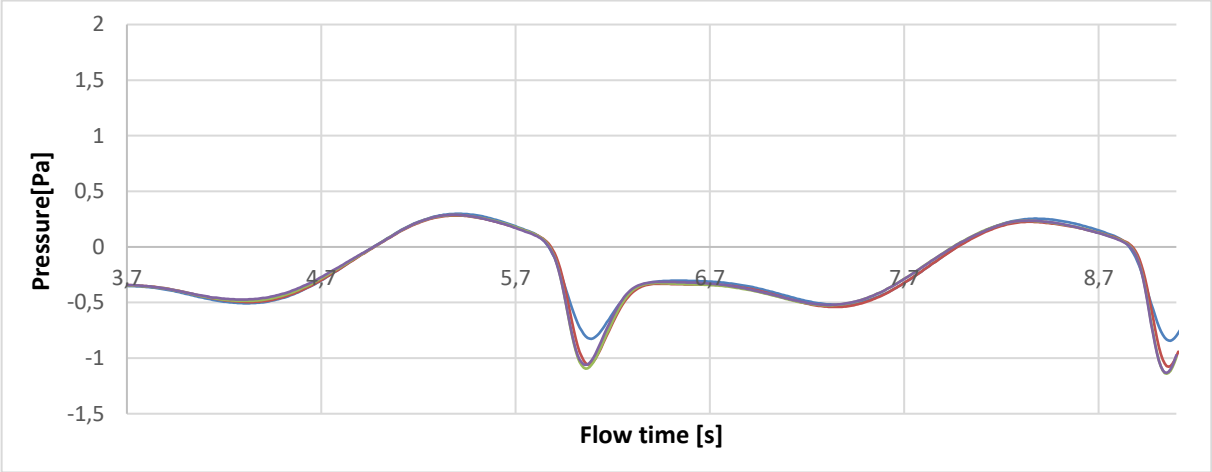

Figure 26.: Pressure values at the outer exit of the duct (blue: Case 1, red: Case 2, yellow: Case 3, purple: Case 4)

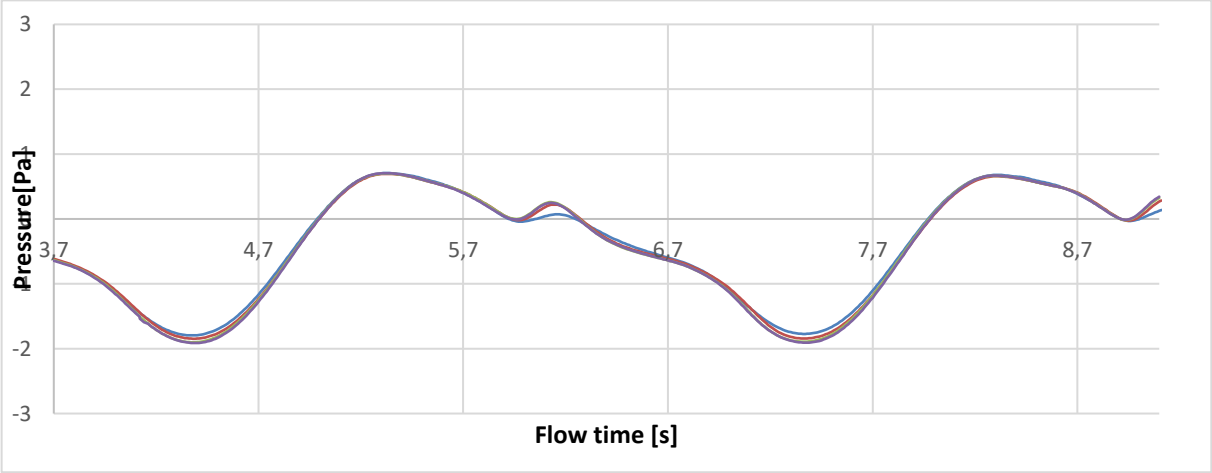

Figure 27.: Pressure values at the orifice (blue: Case 1, red: Case 2, yellow: Case 3, purple: Case 4)

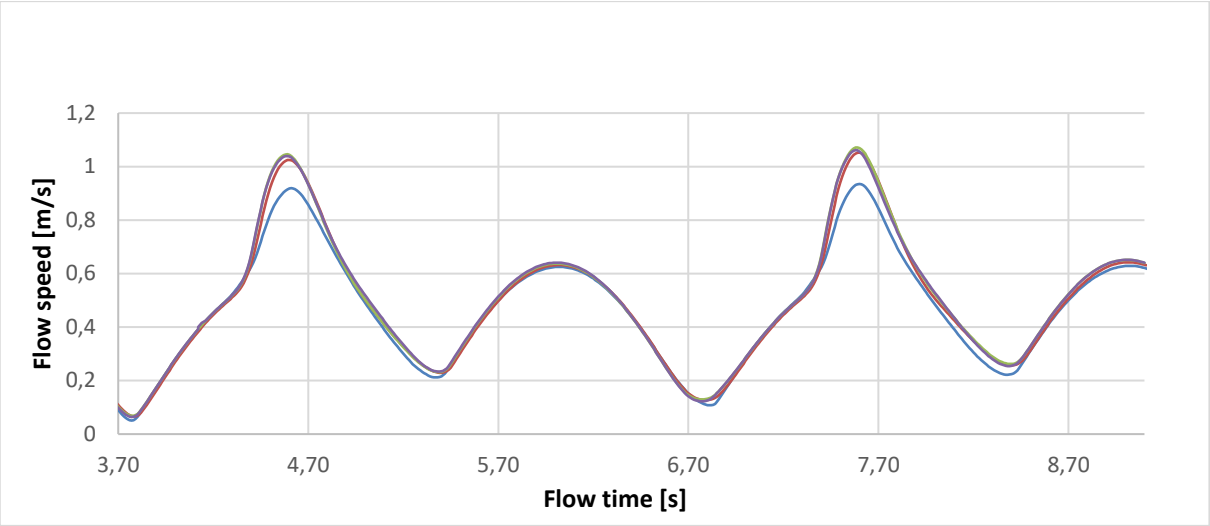

Figure 28.: Flow speed at the inner exit of the duct (blue: Case 1, red: Case 2, yellow: Case 3, purple: Case 4)

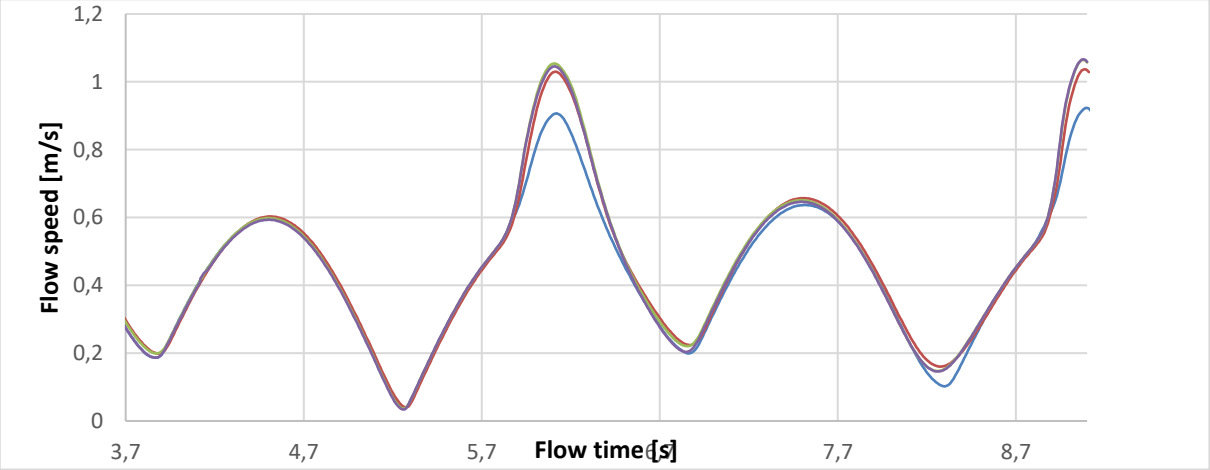

Figure 29.: Flow speed at the outer exit of the duct (blue: Case 1, red: Case 2, yellow: Case 3, purple: Case 4)

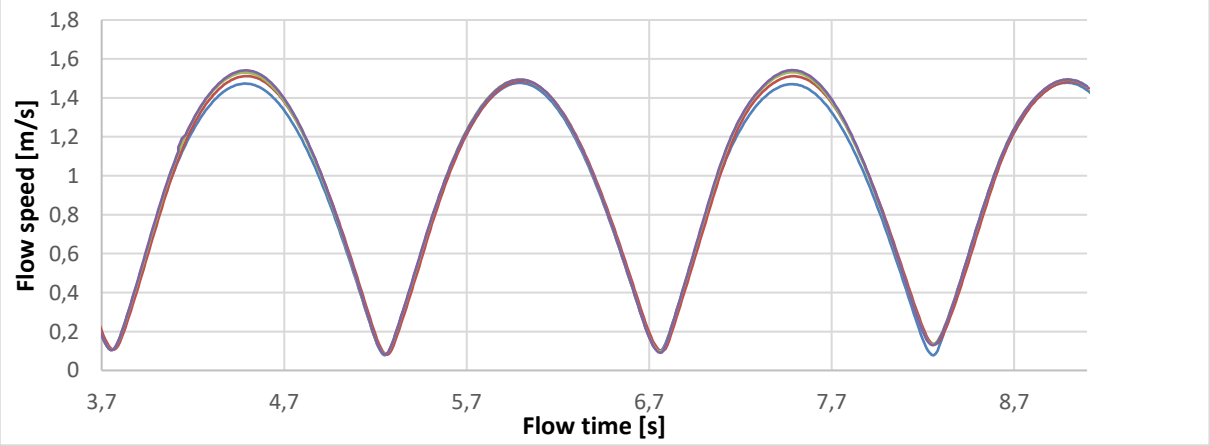

Figure 30.: Flow speed at the orifice (blue: Case 1, red: Case 2, yellow: Case 3, purple: Case 4)

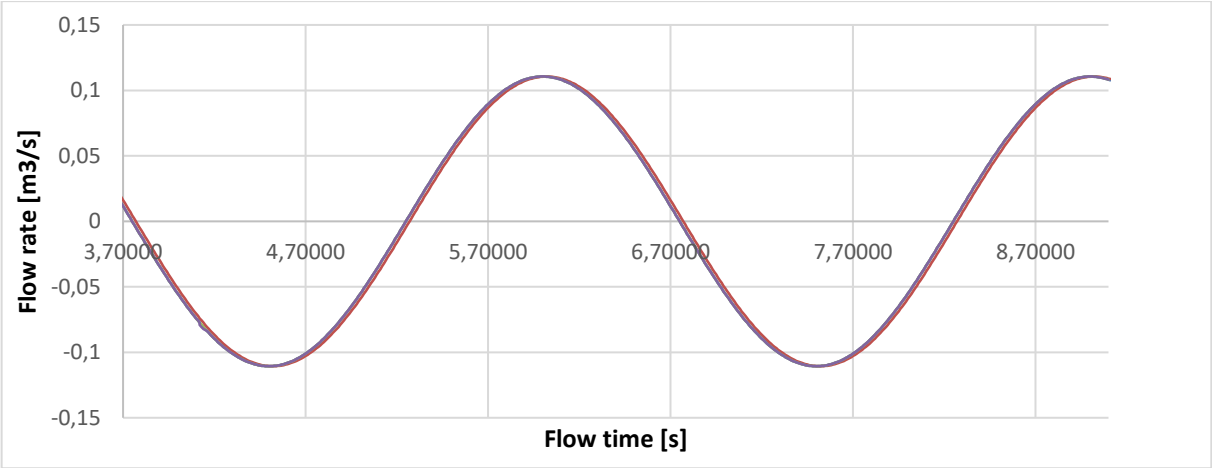

Figure 31.: Volumetric flow rate at the orifice (blue: Case 1, red: Case 2, yellow: Case 3, purple: Case 4)

To find a mesh independent solution a graph showing the flow speed at the outer exit of the duct and the cell number in the duct is shown in Figure 32.

	1. case	2. case	3. case	3. case
Flow speed	1.4766	1.4880	1.4937	1.4941
Cell number in the duct	800	3080	6390	12160

Table 2.: Values of the mesh independent study

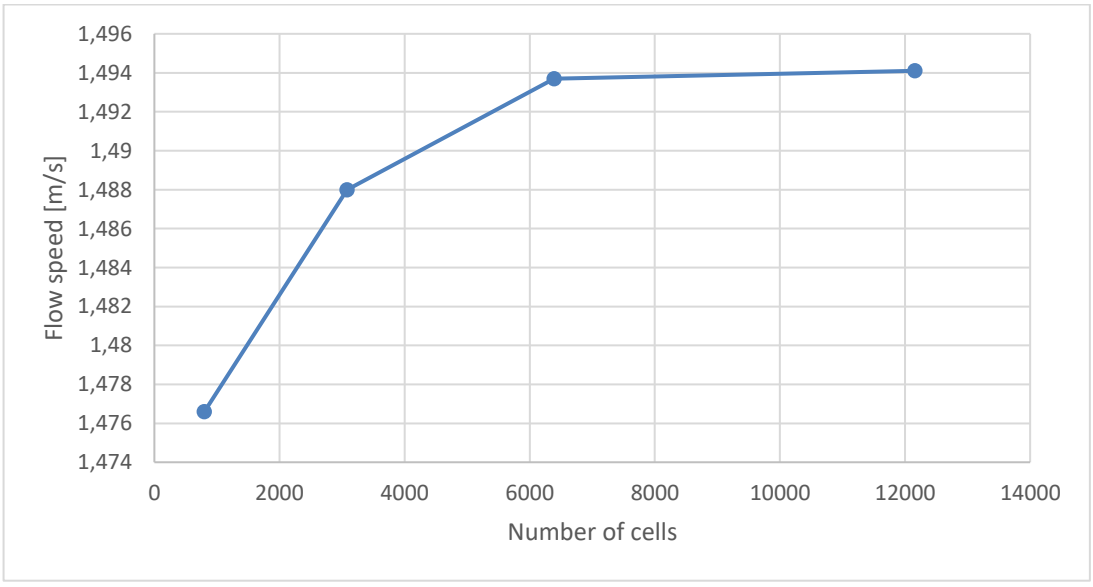

Figure 32.: Graph of the mesh independent study

It is shown on Figure 32. that there is no significant between Case 3 and Case 4, so Case 3 can be presumed satisfactory.

3.2.5. Study of the compressible flow

As the Mach number everywhere inside the chamber is below 0.1, the flow was presumed incompressible. A quick study was performed to confirm the assumption.

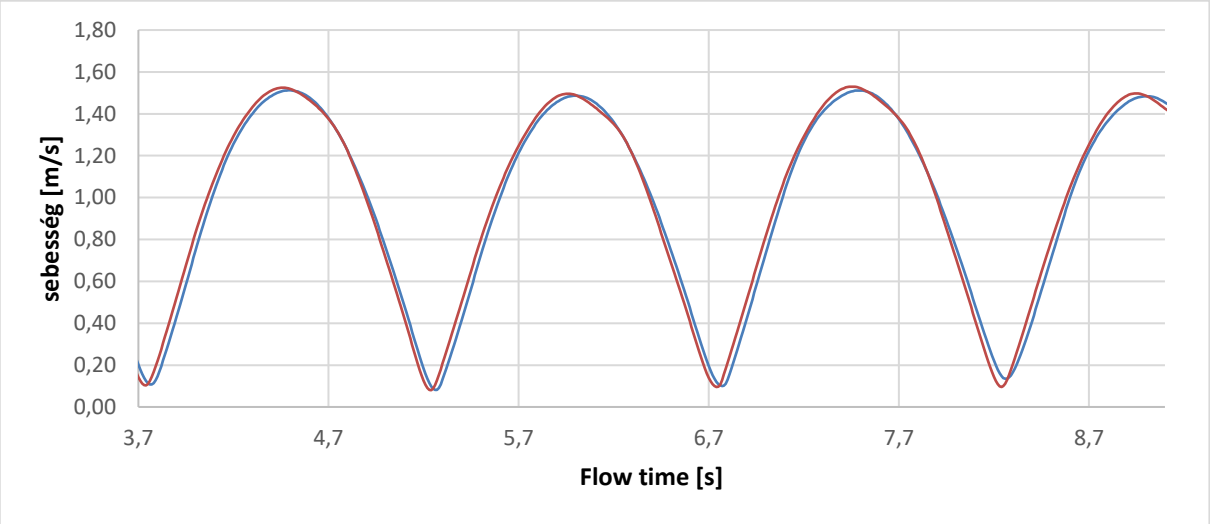

Figure 33.: The flow speed at the orifice (blue: incompressible, red: compressible flow)

As shown on Figure 33. there is no notable difference on the flow speed (~2-3%) and a 0.04 [s] phase swift. This result corresponds with Sarmento and Falcao's study [9]. However, the computational time was increased significantly, so a compressible flow model presumed satisfactory.

3.2.6. Boundary layer inside the chamber.

A study was done on the importance of the boundary layer and found to not affect the flow. Discarding it can further decrease the number of cells in the model.

3.3. Three dimensional Analysis of the OWC Chamber.

In this Section, a three dimensional analysis is described. Section 3.3.1 detailing the importance of the y+ value in the duct. Section 3.3.2 and 3.3.3 shows the current development of the cases with the orifice.

3.3.1. Analysis of the y+ value

The y+ is a non-dimensional wall distance for a wall-bounded flow, which can be defined in the following way:

$$y^+ = \frac{u^* y}{\nu}$$

Where u* is the friction velocity at the nearest wall, y thickness of the first cell and ν is the local kinematic viscosity of the fluid. [24]

For the analysis, a 3D model of the OWC chamber was constructed without an orifice. The meshing was done following the 2D Case 3, shown in Figure 34. The cell number of this model is 177300.

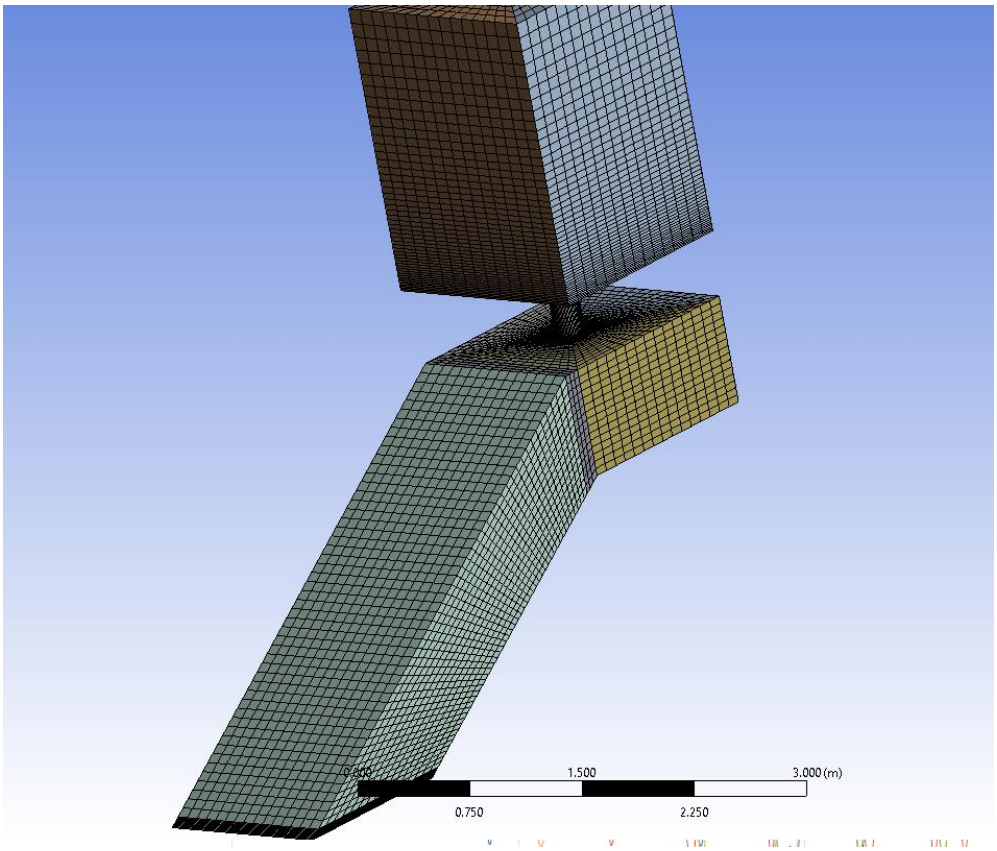

Figure 34.: The mesh of the 3D OWC chamber without an orifice

This first iteration is necessary to calculate an approximate value of the volumetric flow rate. From this the friction velocity is calculated, then with a y^+=1 value, the first cell thickness in the duct is defined. The reason to calculate the friction velocity from the volumetric flow rate, instead of measuring it, is, as shown in the 2D case, that the volumetric flow rate is more mesh independent than other values.

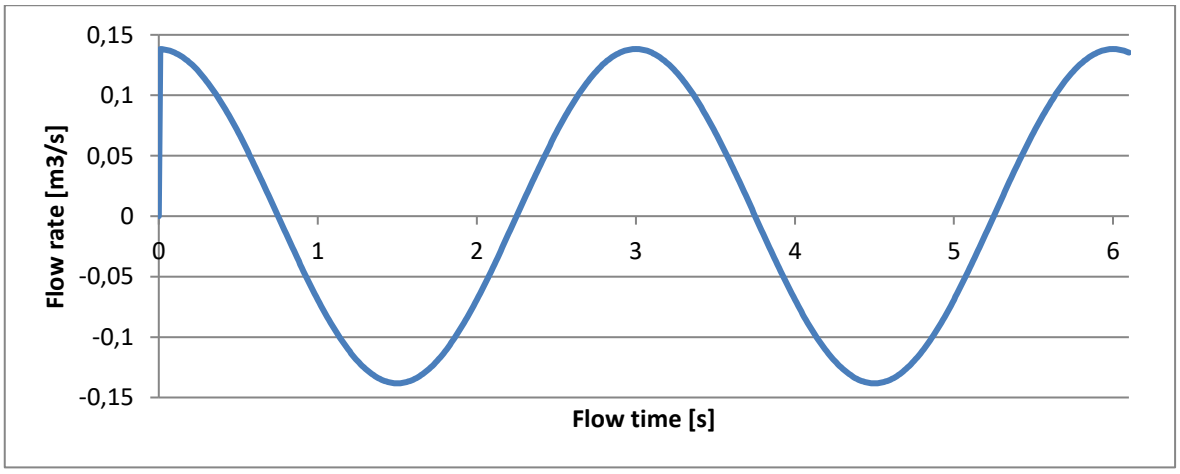

Figure 35.: The volumetric flow rate in the first case.

The maximum volumetric flow rate at 6.00 [s] is 0.1383 [m^3/s], hydraulic diameter is 0.2 [m], so the friction velocity is 0.446 [m/s]. The kinematic viscosity in the simulation is 1.460 [m^2/s], so the first cell thickness is $2.65*10^{-5}$ [m]. The growth rate was set to 1.1, so the cell number of the Case 2 is 1931000.

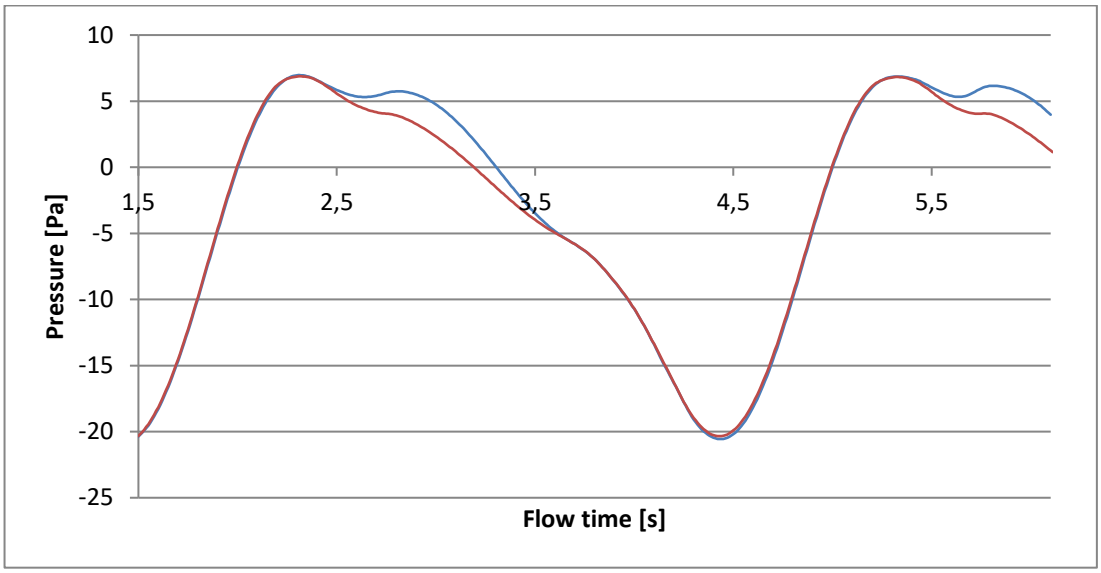

Figure 36.: Pressure values at the inner exit of the duct (blue: first, red: second iteration)

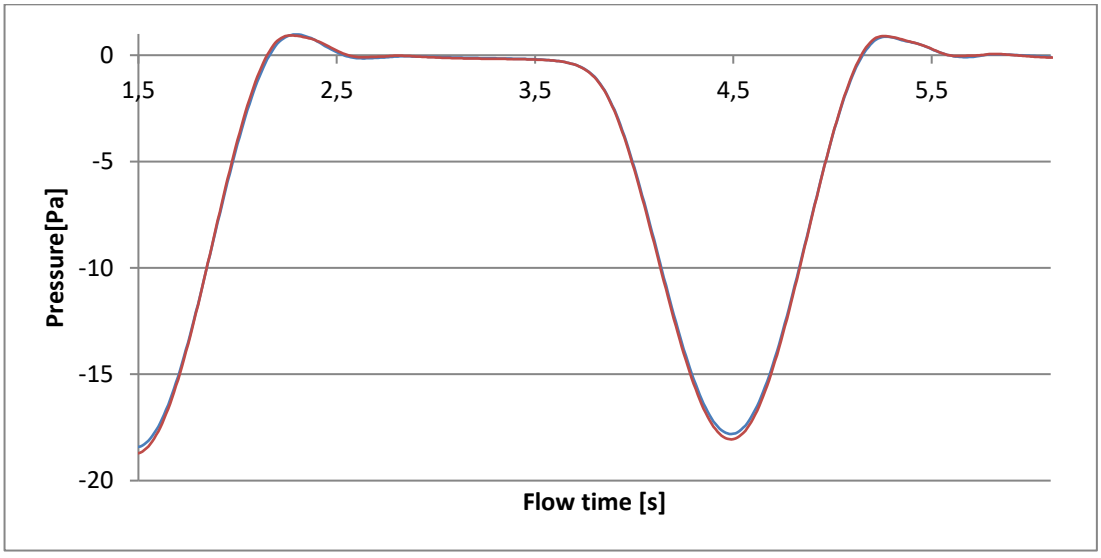

Figure 37.: Pressure values at the outer exit of the duct (blue: first, red: second iteration)

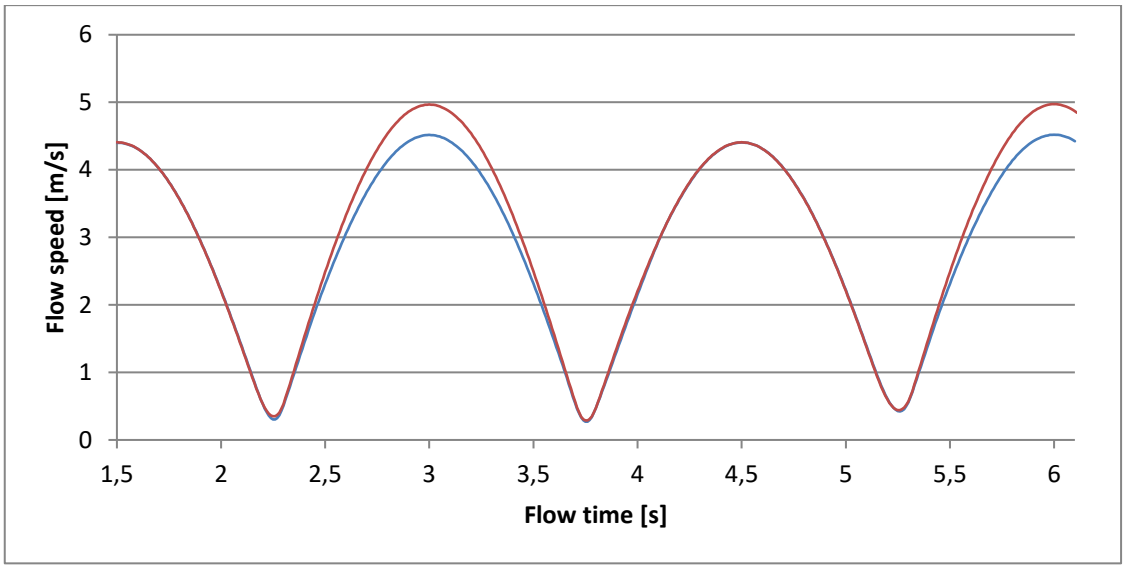

Figure 38.: Flow speed at the inner exit of the duct (blue: first, red: second iteration)

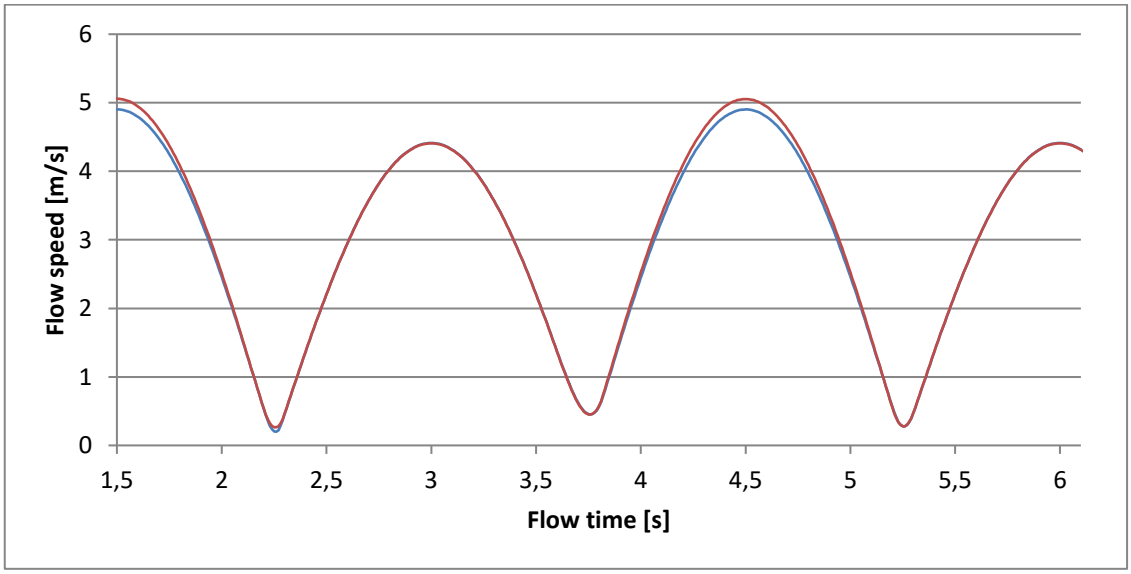

Figure 39.: Flow speed at the inner exit of the duct (blue: first, red: second iteration)

As seen in Figure 38 the difference can be as high as 10%, so the boundary layer inside the duct cannot be discarded.

3.3.2. *Cutcell mesh*

CutCell meshing is a general purpose hex-dominant meshing technique. This method converts the volume mesh into a predominantly Cartesian mesh. Uses some wedges, tetras and pyramids at boundaries to capture the geometry. Used for a quick and easy mesh construction. [23]

This meshing method is not suitable for this geometry, as it can't capture the thin region in the orifice. This results in an inaccurate flow inside the duct, for example the maximum volumetric flow rate was 0.383 [m^3/s], more than twice than in previous models.

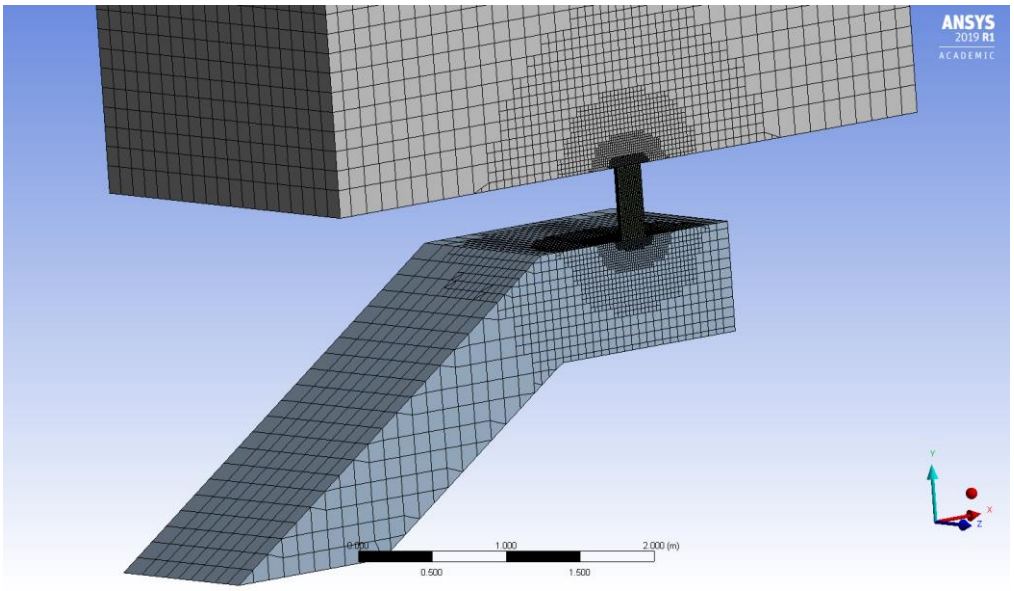

Figure 40.: Cross-section of the CutCell mesh

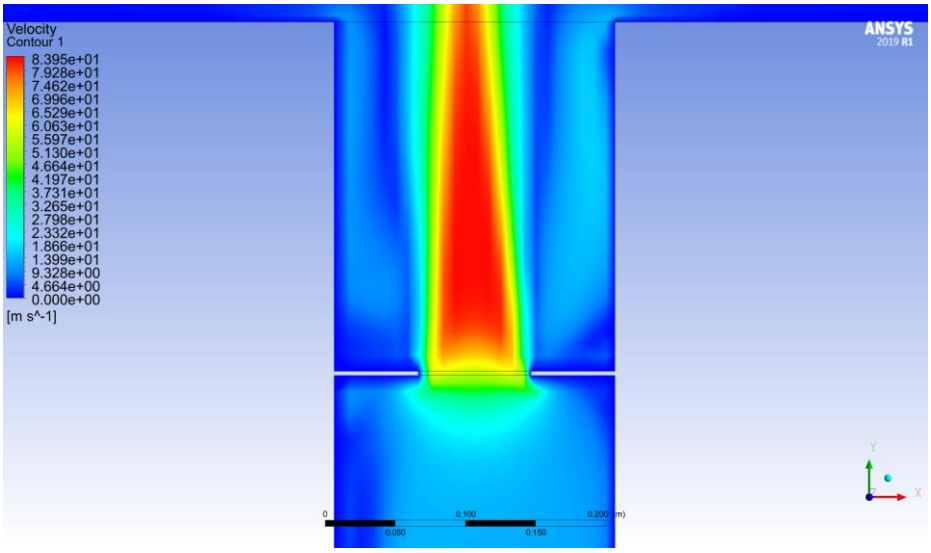

Figure 41.: Velocity contour inside the duct, CutCell mesh

3.3.3. Structured mesh

The mesh construction was done similarly to study detailed in Section 3.3.1. The maximum volumetric flow rate is 0.0202 [m^3/s], thus the first layer thickness on the wall of the duct is $1.401*10^{-4}$ [m].
Four cases will be compared, with various growth rates (1.05, 1.1, 1.15 and 1.2). This comparison is beyond of this thesis's work.

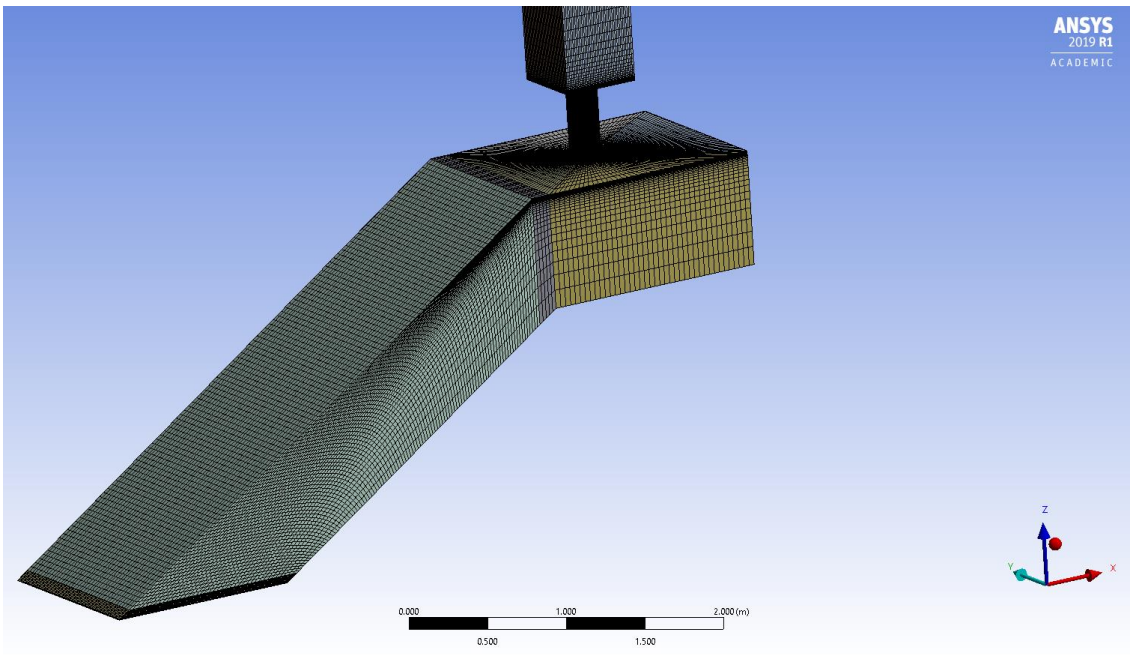

Figure 42.: Isometric view of the 1.2 growth rate mesh

4. CONCLUSIONS

In the first part of this thesis, a research of Oscillating Water Column was done. Detailing the developments throughout the years in experimental and numerical analysis as well. Significant changes were done since the Masuda's navigation bouy, including the introduction of the self-rectifying turbines. The computational testing proved to be an essential part to increase these turbines' efficiency. In the second part, a numerical analysis were conducted using an experimental model geometry, provided by the International Energy Agency– Ocean Energy Systems. First, a two-dimensional study was done, examining the importance of the temporal resolution, incompressible flow and boundary layers. The computational burden is greatly reduced by using a fixed 0.01 [s] time-step, assuming incompressible flow and disregarding the boundary layer in the OWC chamber. In the three-dimensional study the effects of the y+ value was studied, lastly a quicker meshing method was examined. As the thesis details, the y+ value needs to be 1 for the accurate prediction of the flow, so other meshing methods are unsuitable for this problem.

4.1. Further improvements

In this study was a glance in the challenges of the construction of a CFD model. Further improvements can be made with a comparison of the waving water surface and an improved, non-horizontal moving wall. The computational burden can be further reduced with a symmetry plane, cutting the cell size in half. Other wave height and periods should be investigated, resulting a wave independent mesh.

Many more improvements can be done in this subject, regardless of the 70 year history of this technology. Including the optimisation of the chamber geometry, detailed examination of various turbine designs and improving the aeroacoustics of this device.

5. REFERENCES

[1] UNITED STATES PATENT 4,858,434 (1984)

[2] FALCAO A.F.O., HENRIQUES J.C.C. (2016) Oscillating-water-column wave energy converters and air turbine: A review, *Renewable Energy (2016) 1391-1424*

[3] CUI Y., LIU Z., ZHANG X., XU C. (2018) Review of CFD studies on axial-flow self-rectifying turbines for OWC wave energy conversion, *Ocean Engineering 175 (2019) 80-102*

[4] DRESSER-RAND (2015) Oscillating Water Column Technology, HydroAir Turbine, *Form 15002-15*

[5] SETOGUCHI T., TAKAO M. (2005) Current status of self rectifying air turbines for energy conversion, *Energy Conversion and Management 47 (2006) 2382-2396*

[6] HU H.H. (2012) Fluid Mechanics, Chapter 10, Computational Fluid Dynamics

[7] REYNOLDS O. (1894) On the Dynamical Theory of Incompressible Viscous Fluids and the Determination of the Criterion

[8] ANSYS THEORY GUIDE

[9] SARMENTO A.J.N.A., FALCAO A.F.O. (1985) Wave generation by an oscillating surface-pressure and its application in wave-energy extraction, *Journal of Fluid Mechanics (1985) vol.150, 467-485*

[10] WATTERSON J.K., RAGHUNATHAN S. (1996) Investigation of Wells Turbine Performance using 3-D CFD

[11] TORESSI M., CAMPOREALE S.M., STRIPPOLI P.D., PASCAZIO G. (2007) Accurate numerical simulation of a high solidity Wells turbine, *Renewable Energy 33 (2008) 735-747*

[12] CUI Y., HYUN B-S (2015) Numerical study on Wells turbine with penetrating blade tip treatments for wave energy conversion, *International Journal of Naval Architecture and Ocean Engineering (2016) 1-10*

[13] THAKKER A., FRAWLEY P., KHALEEQ H.B., ABUGIHALIA Y. (2001) Experimental and CFD Analysis of 0.6m Impulse Turbine with Fixed Guide Vanes, *Proceedings of the Eleventh (2001) International Offshore and Polar Engineering Conference*

[14] TAKAO M., THAKKER A., ABDULHADI R., SETOGUCHI T. (2006) Effect of blade profile on the performance of a large-scale Wells-turbine for wave-energy conversion, *International Journal of Sustainable Energy (2006) Vol. 25, 53-61*

[15] AHMED Y.M., MAZUKEE U.J.A., YAAKOB O.B., ELBATRAN A.H. (2015) Wells Turbine for Wave Energy Conversion for Malaysian Ocean, *Journal of Ocean, Mechanicaal and Aerospace, Vol.6*

[16] MOHAMED M.H.A. (2011) Design optimization of Savonius and Wells Turbines

[17] WATTERSON J.K., RAGHUNATHAN S. (1998) Computed Effects of Solidity on Wells Turbine Performance

[18] HALDER P., RHEE S.H., SAMAD A. (2016) Numerical optimization of Wells turbine for wave energy extraction, *International Journal of Naval Architecture and Ocean Engineering (2016) 11-24*

[19] TORRESI M., CAMPOREALE S.M., PASCAZIO G., FORTUNATO B. (2004) Fluid Dynamic Analysis of a Low Solidity Wells Turbine

[20] TAHA Z., SUGIYOGO, TUAN YA T.M.Y.S., SAWADA T. (2011) Numerical investigation on the performance of Wells turbine with non-uniform tip clearance for wave energy conversion, *Applied Ocean Research 33 (2011) 321-331*

[21] CUI Y., HYUN B-S. (2016) Numerical study on Wells turbine with penetrating blade tip treatments for wave energy conversion, *International Journal of Naval Architecture and Ocean Engineering (2016) 1-10*

[22] PARK S., KIM K-H., NAM B-W., KIM J-S., HONG K. (2019) Experimental and Numerical Analysis of Performance of Oscillating Water Column Wave Energy Converter Applicable to Breakwaters, *Proceedings of the ASME 2019 38th International Conference on Ocean, Offshore and Arctic Engineering*

[23] https://cfd.ninja/ansys-meshing-cutcell/ (2019)

[24] https://wiki.uiowa.edu/display/greenergy/Oscillating+Water+Column (2019)

[25] https://www.cfd-online.com/Wiki/Dimensionless_wall_distance_(y_plus) (2019)